



Embedding short-range correlations in relativistic density functionals through quasi-deuterons

S. Burrello^{1,a}, S. Typel^{1,2,b}

¹ Technische Universität Darmstadt, Fachbereich Physik, Institut für Kernphysik, Schlossgartenstraße 9, 64289 Darmstadt, Germany

² GSI Helmholtzzentrum für Schwerionenforschung GmbH, Theorie, Planckstraße 1, 64291 Darmstadt, Germany

Received: 1 April 2022 / Accepted: 12 June 2022

© The Author(s) 2022

Communicated by Vittorio Somà

Abstract The formation of clusters at sub-saturation densities, as a result of many-body correlations, constitutes an essential feature for a reliable modelization of the nuclear matter equation of state (EoS). Phenomenological models that make use of energy density functionals (EDFs) offer a convenient approach to account for the presence of these bound states of nucleons when introduced as additional degrees of freedom. However, in these models clusters dissolve, by construction, when the nuclear saturation density is approached from below, revealing inconsistencies with recent findings that evidence the existence of short-range correlations (SRCs) even at larger densities. The idea of this work is to incorporate SRCs in established models for the EoS, in light of the importance of these features for the description of heavy-ion collisions, nuclear structure and in the astrophysical context. Our aim is to describe SRCs at supra-saturation densities by using effective quasi-clusters immersed in dense matter as a surrogate for correlations, in a regime where cluster dissolution is usually predicted in phenomenological models. Within the EDF framework, we explore a novel approach to embed SRCs within a relativistic mean-field model with density dependent couplings through the introduction of suitable in-medium modifications of the cluster properties, in particular their binding energy shifts, which are responsible for describing the cluster dissolution. As a first exploratory step, the example of a quasi-deuteron within the generalized relativistic density functional approach is investigated. The zero temperature case is examined, where the deuteron fraction is given by the density of a boson condensate. For the first time, suitable parameterizations of the cluster mass shift at zero temperature are derived for all baryon densities. They are constrained by experimental results for the effective deuteron

fraction in nuclear matter near saturation and by microscopic many-body calculations in the low-density limit. A proper description of well-constrained nuclear matter quantities at saturation is kept through a refit of the nucleon meson coupling strengths. The proposed parameterizations allow to also determine the density dependence of the quasi-deuteron mass fraction at arbitrary isospin asymmetries. The strength of the deuteron-meson couplings is assessed to be of crucial importance. Novel effects on some thermodynamic quantities, such as the matter incompressibility, the symmetry energy and its slope, are finally discerned and discussed. The findings of the present study represent a first step to improve the description of nuclear matter and its EoS at supra-saturation densities in EDFs by considering correlations in an effective way. In a next step, the single-particle momentum distributions in nuclear matter can be explored using proper wave functions of the quasi-deuteron in the medium. The momentum distributions are expected to exhibit a high-momentum tail, as observed in the experimental study of SRCs by nucleon knockout with high-energy electrons. This will be studied in a forthcoming publication with an extensive presentation of the theoretical method and the results.

1 Introduction

The Equation of State (EoS) of strongly interacting matter is a fundamental ingredient in the theoretical description of compact stars. It plays also a crucial role in many astrophysical simulations of, e.g., core-collapse supernovae and neutron star mergers [1–4]. Tight links have been also established between the properties of the EoS and those of finite nuclei, concerning both their structure and reaction dynamics [5–7]. A large variety of approaches has been employed therefore in the last decades to develop reliable models for the EoS, which are constrained by both nuclear physics

^a e-mail: burrello@lns.infn.it

^b e-mail: stypel@ikp.tu-darmstadt.de (corresponding author)

experiments and astronomical observations. For astrophysical simulations, tables of global, multi-purpose EoSs are in particular needed, being provided by sophisticated theoretical methods available in literature [8].

One class is given by microscopic ab-initio models, which try to solve the nuclear many-body problem using advanced methods and realistic interactions that are constrained by scattering data and properties of few-nucleon systems, see, e.g., Refs. [9,10]. Other approaches based on the effective-field theory exploit systematic developments from quantum chromodynamics and symmetry concepts, e.g. in chiral perturbation theory, providing also uncertainty estimates [11–13]. However, these models fail in properly describing the formation of clusters at densities below nuclear saturation, where these bound states of nucleons emerge as many-body correlations generated by the short-range nucleon-nucleon interaction. Such low-density conditions are encountered in various systems: the debris of heavy-ion collisions (HIC), the post-bounce evolution of core-collapse supernovae, and the surface of nuclei [14,15] where the formation of clusters is a prerequisite for cluster radioactivity and, in particular, α -decay of heavy nuclei. The emergence of clusters is definitely an essential feature for the modelization of a realistic EoS [16].

Phenomenological models, whose parameters are constrained from experimental results of HIC and astronomical observations and/or by directly fitting properties of finite nuclei and nuclear matter near saturation, offer a convenient alternative to microscopic models to approach this problem. A widely used class of phenomenological approaches is based on energy density functionals (EDFs), which are usually derived in the self-consistent mean-field approximation with an effective in-medium interaction without a direct connection to the nucleon-nucleon interaction in free space [17]. There are various versions of this approach, e.g., non-relativistic models using Skyrme or Gogny type interactions [18,19] or relativistic models based on the exchange of mesons [20]. In recent years, several attempts have been made to also directly link EDFs to microscopic ingredients [21–23]. For example, a special class of functionals inspired by effective field theories (EFTs) and bench-marked on ab-initio predictions have been designed [24,25]. They were applied to finite nuclei [26] and finite temperature EoS calculations of pure neutron matter (PNM) [27]. Moreover, few steps were made towards the construction of a power counting in EDF [28,29].

However, EDFs derived from phenomenological mean-field models fail as well, when only nucleons are considered as basic constituents. Further progress is only achieved if clusters are introduced as additional explicit degrees of freedom at low densities [30]. The dilute matter is then depicted as an ideal mixture of nucleons and all nuclei from the table of isotopes in thermodynamic equilibrium. Such a model is

called nuclear statistical equilibrium (NSE) and is widely used in the astrophysical context, where it leads to a reliable description for the chemical composition of stellar matter at sub-saturation densities [16,31]. However, models like NSE are considered valid only as long as the interaction between the constituents can be neglected. Thus they fail at higher densities where in-medium effects become important, leading to the dissolution of clusters and the transition to cluster-free nuclear matter. The dissolution of a cluster, i.e., the so-called Mott effect, which is expected when approaching nuclear saturation density from below, can be produced through the introduction of an excluded-volume mechanism, which is just a simple geometric concept [16,32–34]. More microscopically, the formation and dissolution of light clusters in nuclear matter can be treated using a quantum statistical approach with thermodynamic Green's functions, see, e.g., Refs. [35,36].

An alternative scenario was proposed in the last decade, when interacting clusters were introduced as explicit degrees in relativistic density functionals, firstly concentrating on light hydrogen and helium isotopes, whose properties are modified in the medium [30]. Contrary to the chemical picture traditionally adopted in NSE-like models, where the properties of the correlated states of nucleons are assumed to be independent of the medium, in such a physical picture, the in-medium effects are addressed by introducing a proper modification of the masses of the clusters, as inspired by the quantum statistical approach. Following this idea, the effective binding energies are expected to decrease with density [37].

Many-nucleon correlations in the continuum, which still survive above the Mott density, are then described in terms of effective resonances or quasi-clusters. In current phenomenological approaches with the excluded-volume mechanism or with medium-dependent mass shifts, these states are statistically suppressed by construction beyond saturation, so that only nucleons should remain as independent quasi-particles [38]. Mean-field type descriptions of nuclear matter above saturation consider thus the system as a free Fermi gas, with the usual step function in the single-particle momentum distribution at zero temperature. Such a picture is however inconsistent with recent experimental results from nucleon knock-out reactions on nuclei using inelastic electron scattering [39,40]. These studies clearly evidence the smearing of the nucleon Fermi surface and the emergence a high-momentum tail (HMT) in the single-nucleon momentum distribution of cold nucleonic matter, ascribable to the existence of sizeable nucleon-nucleon short-range correlations (SRCs) even at saturation density [40–42].

Experimental investigations assessed that SRCs pairs are formed by approximately 20% of nucleons in various measured nuclei [43–45]. They are characterized by large relative and small center-of-mass (c.m.) momenta. Moreover,

some results concluded that their magnitude is spin- and isospin-dependent, with a clear dominance in the neutron-proton channel [44–47], that affects the ratio of minority and majority species in asymmetric nuclear matter, in the bulk part and tail of the single-particle momentum distributions [46, 48]. Extrapolating these experimental results from finite nuclei to infinite nuclear matter, useful information around saturation density was then deduced. At higher densities, only numerical investigations exist to predict the density dependence of these SRC pairs. From the analysis, the probability for nucleons to form SRC pairs seems to have a minimum in the neighbourhood of the saturation density, owing to the interplay between the tensor component and the repulsive core of the nuclear force [49–51].

SRCs may also change the balance between kinetic and potential contributions to the energy of the system. Thus their introduction is expected to significantly affect the controversial density dependence, in particular at supra-saturation densities, of the nuclear symmetry energy [52, 53], which quantifies the difference between the total energy of PNM and symmetric nuclear matter (SNM). Many theoretical and experimental investigations are currently investigating the density dependence of this quantity [54–58].

The purpose of the present work is to incorporate SRCs in established models for the EoS, in light of the key-importance of these features for the description of HIC, nuclear structure and in the astrophysical context [59–62]. Our aim is to explicitly treat SRCs at supra-saturation densities by using effective quasi-clusters immersed in dense matter as a surrogate for correlations, through the introduction of proper in-medium modifications of the cluster mass shifts. In this regime cluster dissolution is usually predicted in actual realizations of phenomenological models. Within the EDF framework, we propose thus a novel approach to embed the SRCs within a relativistic mean-field model (RMF) with density dependent couplings [63] through a substantial modification of the cluster mass shift at high densities.

Given its phenomenological nature, the adopted approach does not allow to investigate the origin of the SRCs. Several effects coexist in the high-density regime that can lead to a smearing of the single-particle distribution functions and the appearance of HMTs as known from the description of heavy-ion collisions in transport theory [64]. They are due to different (repulsive) components of the nucleon-nucleon interaction and can be hardly disentangled. A deeper insight on these features would indeed require a more microscopic treatment of these SRCs, going beyond the scope of the present work.

As a first exploratory step, the example of a quasi-deuteron within this generalized relativistic density functional (GRDF) is currently explored, since two-body SRCs in the neutron-proton 3S_1 channel are much more important than other many-body correlations. The zero tempera-

ture case is examined, where the deuteron is represented by a boson condensate that determines the mass fraction and leads to specific conditions to the parameterization of the mass shift. The purpose of this work is then to propose possible mass shift parameterizations that will be employed to determine the density dependence of the quasi-deuteron mass fraction at arbitrary isospin asymmetries. The final ambitious goal is to investigate the effect of accounting for the SRCs in an effective way on the EoS, and some related thermodynamic quantities, at supra-saturation densities. In this context, it is worthwhile to mention that a recent study employed the concept of a mass shift in a similar approach to model the effective interaction of a possible heavy particle with baryon number $B = 2$, the so-called *seaquark*, in nuclear matter. It is treated as a boson condensate like the deuteron and affects the EoS of compact-star matter and thus the properties of neutron stars [65].

The present work concentrates on the relation between the parameterisation of the cluster mass shift and the quasi-deuteron mass fraction. The investigation of the single-nucleon momentum distribution requires to determine the quasi-deuteron wave function in the medium. The corresponding self-consistent approach and the results will be presented in detail in a future publication.

The manuscript is structured as follows. In Sect. 2 the theoretical formalism is illustrated and the fundamental principles and basic formulas of the GRDF are given. The case of zero temperature is studied, where quasi-deuteron condensation is expected, and the role of the deuteron-meson coupling strength is discussed. Section 3 explores the different constraints for the deuteron mass shifts. Section 4 concentrates on the mass shift parameterization, as suitably derived for nuclear matter at zero temperature. Then, the corresponding density dependence of the quasi-deuteron mass fraction is obtained. The impact on the EoS and on some general properties of nuclear matter at arbitrary neutron-proton asymmetries is shown in Sect. 5. Conclusions and an outlook are finally given in Sect. 6. Details on the formal derivation of some quantities, on the conversion of parameters and analytical expressions for the mass shift parameters are furthermore collected in four appendices.

2 Theoretical formalism

2.1 Generalized relativistic density functional

The GRDF is a density functional derived from a RMF with nucleons and further degrees of freedom. Their effective interaction in the medium is described by the exchange of mesons with density dependent couplings [30, 63]. In such a model, light clusters are explicitly introduced, allowing for a unified treatment from matter with bound nucleons at low

densities to matter possibly made of only neutrons (n) and protons (p) at high densities. All degrees of freedom are represented by quasi-particles with self-energies that incorporate the effects of the interaction. For sake of simplicity, only ^2H nuclei (labeled as d in the following) are added to nucleons as degrees of freedom in light of their expected prevalent importance discussed in Sect. 1.

Let us thus consider the general case of asymmetric nuclear matter (ANM) composed of neutrons, protons and deuterons with particle number densities n_i ($i = n, p, d$), baryon numbers A_i and charge numbers Z_i . The system is usually characterized by specifying the baryon density $n_b = n_n + n_p + 2n_d$, the isospin asymmetry $\beta = (n_n - n_p)/n_b$ and the temperature T . In this section, the basic formulas of the theoretical formalism are given for the most general case of finite temperature. However, the zero temperature case will be considered in the analysis performed in the following sections, leaving the analysis at finite T for future work. In this work, the masses of neutrons and protons will be taken as equal to the average nucleon mass m_{nuc} so that $m_n = m_p = m_{\text{nuc}}$. The same values as given in Ref. [30] are considered.

Following the framework illustrated in Refs. [38, 66], the thermodynamic properties of nuclear matter are completely determined once the grand canonical potential density $\tilde{\omega}(T, \{\mu_i\})$ is specified. It depends, apart from the temperature, on the chemical potentials μ_i of all constituents i . In the present work, three types of mesons are considered: an isoscalar scalar σ meson to describe the attraction between nucleons, an isoscalar vector ω meson for their repulsion and an isovector vector ρ meson for the isospin dependence of the strong force. The interaction between a baryon i and a meson j ($j = \sigma, \omega, \rho$) is realized by a minimal coupling with a strength that is given by the product of a scaling factor χ_{ij} , the mass number A_i , and a coupling Γ_j . The latter quantity depends on the baryon density n_b to describe the medium dependence of the effective interaction. Different prescriptions might be adopted as recently discussed in Ref. [67]. In this work the functional form of the couplings as introduced in Ref. [63] is used. In the application of the GRDF to homogeneous nuclear matter, only the ratio Γ_j/m_j of coupling and mass m_j of the mesons j is relevant. Hence it is convenient to introduce the coefficients

$$C_j = \frac{\Gamma_j^2}{m_j^2} \quad (1)$$

and their derivatives

$$C'_j = \frac{dC_j}{dn_b} = 2 \frac{\Gamma_j}{m_j^2} \frac{d\Gamma_j}{dn_b} \quad (2)$$

with respect to the baryon density.

The total grand canonical potential density of the system can be written as

$$\tilde{\omega}(T, \{\mu_i\}) = \sum_i \tilde{\omega}_i + \tilde{\omega}_d^{(\text{cond})} + \tilde{\omega}_{\text{meson}} - \tilde{\omega}_{\text{meson}}^{(\text{r})} \quad (3)$$

containing the standard expression for the single quasi-particle (non-mesonic) contribution

$$\tilde{\omega}_i = -T \frac{g_i}{\sigma_i} \int \frac{d^3k}{(2\pi)^3} \ln \left[1 + \sigma_i \exp \left(-\frac{E_i - \mu_i^*}{T} \right) \right] \quad (4)$$

with the well-known integral over the momentum k that appears in the quasi-particle energy

$$E_i = \sqrt{k^2 + (m_i^*)^2} \quad (5)$$

assuming natural units such that $\hbar = c = 1$. In Eq. (4), the sign factor σ_i distinguishes the particle statistics ($\sigma_i = 1$ for fermions and $\sigma_i = -1$ for bosons, respectively) and g_i is the spin-degeneracy factor. The boson condensate term

$$\tilde{\omega}_d^{(\text{cond})} = \frac{1 - \sigma_d}{2} n_d^{(\text{cond})} (m_d^* - \mu_d^*) \quad (6)$$

in Eq. (3) with the density of the condensate, $n_d^{(\text{cond})}$, is only relevant for deuterons.

The effective chemical potential

$$\mu_i^* = \mu_i - V_i. \quad (7)$$

and the effective mass

$$m_i^* = m_i + \Delta m_i - S_i \quad (8)$$

depend on scalar

$$S_i = \chi_{i\sigma} A_i C_\sigma n_\sigma \quad (9)$$

and vector

$$V_i = \chi_{i\omega} A_i C_\omega n_\omega + \chi_{i\rho} A_i C_\rho n_\rho + A_i V^{(r)} + W_i^{(r)} \quad (10)$$

potentials, respectively. They are defined in terms of the different source densities

$$n_\sigma = \sum_i \chi_{i\sigma} A_i n_i^{(s)} \quad (11)$$

$$n_\omega = \sum_i \chi_{i\omega} A_i n_i^{(v)} \quad (12)$$

$$n_\rho = \sum_i \chi_{i\rho} A_i n_i^{(v)} \quad (13)$$

where the single-particle scalar densities ($n_i^{(s)}$) and vector densities ($n_i^{(v)}$) appear.

The mass shift Δm_i in the effective mass (8) appears only for the deuteron and is assumed to depend on the baryon density n_b . This dependence leads to a rearrangement contribution

$$W_i^{(r)} = n_d^{(s)} \frac{\partial \Delta m_d}{\partial n_i^{(v)}} \quad (14)$$

in the vector potentials (10) of nucleons and the deuteron.

The further rearrangement contribution

$$V^{(r)} = \frac{1}{2} \left(C'_\omega n_\omega^2 + C'_\rho n_\rho^2 - C'_\sigma n_\sigma^2 \right) \quad (15)$$

in the vector potential (10) is due to the density dependence of the couplings Γ_j and can be expressed with the coefficients C_j and source densities n_j of the three mesons considered here.

Corresponding to the two rearrangement contribution in (10), there are also two such terms in the total grand potential density (3): the meson term

$$\tilde{\omega}_{\text{meson}}^{(r)} = V^{(r)} n_b \quad (16)$$

and the mass shift term

$$\tilde{\omega}_{\text{mass}}^{(r)} = \sum_i n_i^{(v)} W_i^{(r)} \quad (17)$$

Furthermore, the meson contribution in (3) is given by

$$\tilde{\omega}_{\text{meson}} = -\frac{1}{2} \left(C_\omega n_\omega^2 + C_\rho n_\rho^2 - C_\sigma n_\sigma^2 \right) \quad (18)$$

similar in structure to (15).

The single-particle number densities can be derived from (3) using the thermodynamic definitions

$$n_i^{(v)} = -\frac{\partial \tilde{\omega}}{\partial \mu_i} \Big|_{T, \{\mu_j\}_{j \neq i}} \quad (19)$$

$$n_i^{(s)} = \frac{\partial \tilde{\omega}}{\partial m_i} \Big|_{T, \{\mu_j\}} \quad (20)$$

that give

$$n_i^{(v)} = g_i \int \frac{d^3 k}{(2\pi)^3} d_i + \frac{1 - \sigma_i}{2} n_i^{(\text{cond})} \quad (21)$$

$$n_i^{(s)} = g_i \int \frac{d^3 k}{(2\pi)^3} \frac{m_i^*}{E_i} d_i + \frac{1 - \sigma_i}{2} n_i^{(\text{cond})} \quad (22)$$

with a thermal and a condensate contribution, once the distribution function

$$d_i(T, k, m_i^*, \mu_i^*) = \left[\exp \left(\frac{E_i - \mu_i^*}{T} \right) + \sigma_i \right]^{-1} \quad (23)$$

is defined. These expressions are consistent with the usual definitions of the densities. The vector densities can be expressed as

$$n_n^{(v)} = \frac{1 + \beta - X_d}{2} n_b \quad (24)$$

$$n_p^{(v)} = \frac{1 - \beta - X_d}{2} n_b \quad (25)$$

$$n_d^{(v)} = \frac{X_d}{2} n_b \quad (26)$$

using the baryon density n_b , the asymmetry β , and the deuteron fraction X_d .

The deuteron fraction has to stay below a maximum value of

$$X_d^{(\text{max})} = \frac{m_{\text{nuc}}}{\chi C_\sigma n_b} \quad (27)$$

in order to ensure positive effective masses of the nucleons. This limit is reached when the effective masses of the nucleons are zero, i.e., $S_n = S_p = C_\sigma n_\sigma = m_{\text{nuc}}$ with the source density $n_\sigma = 2\chi n_d^{(s)} = \chi X_d^{(\text{max})} n_b$ of the σ meson. It only has a contribution from the quasi-deuterons because the scalar densities of the nucleons vanish for $m_{\text{nuc}}^* = 0$. A second limitation of the deuteron fraction arises from the fact that for every neutron a proton is needed, or vice versa, to form the cluster. This translates to the condition $X_d \leq 1 - |\beta|$ depending on the isospin asymmetry β . So, in total, one has $0 \leq X_d \leq \min \{ X_d^{(\text{max})}, 1 - |\beta| \}$.

At high densities or temperatures, a mixture of deuterons, neutrons and protons might be expected. If all three particle species have non-zero densities, the condition of chemical equilibrium

$$\mu_d = \mu_n + \mu_p, \quad (28)$$

applies between the chemical potentials of the degrees of freedom involved. Using the definitions (7) and (8) with the potentials (9) and (10), this relation can be written as

$$\Delta m_d = \mu_n^* + \mu_p^* - m_d + S_d + V_n + V_p - V_d, \quad (29)$$

and thus an expression for the deuteron mass shift is obtained.

All thermodynamic quantities of the system can be easily obtained from the grand canonical thermodynamic potential (3). For instance, the pressure is given by

$$P = -\omega(T, \{\mu_i\}) \quad (30)$$

and the free energy density \mathcal{F} can be expressed as

$$\mathcal{F} = \sum_{i=n, p, d} \mu_i n_i^{(v)} + \omega = \left(\mu_b + \frac{1 - \beta}{2} \mu_c \right) n_b - P \quad (31)$$

with the baryon chemical potential $\mu_b = \mu_n$ and the charge chemical potential $\mu_c = \mu_p - \mu_n$. The entropy density finally can be written as

$$\begin{aligned} S &= -\frac{\partial \omega}{\partial T} \Big|_{\{\mu_i\}} + S_{\text{cond}} \\ &= -\sum_i g_i \int \frac{d^3 k}{(2\pi)^3} \left[d_i \ln d_i + \frac{1 - \sigma_i d_i}{\sigma_i} \ln (1 - \sigma_i d_i) \right] \\ &\quad + n_d^{(\text{cond})} \ln g_d \end{aligned} \quad (32)$$

with the distribution functions (23) and a contribution of the condensed deuterons. The latter contribution arises because deuterons have spin 1 and thus the ground state of nuclear matter at $T = 0$ contains a mixture of the different spin substates.

2.2 Zero temperature and quasi-deuteron condensation

If the temperature vanishes, the vector and scalar densities of the nucleons $q = n, p$ can be expressed in analytical form as

$$n_q^{(v)} = \frac{g_q}{6\pi^2} k_q^3 \quad (33)$$

with $g_q = 2$ and

$$n_q^{(s)} = \frac{g_q m_q^*}{4\pi^2} \left[k_q \mu_q^* - (m_q^*)^2 \ln \frac{k_q + \mu_q^*}{m_q^*} \right] \quad (34)$$

with the Fermi momentum k_q and the effective chemical potential

$$\mu_q^* = \sqrt{k_q^2 + (m_q^*)^2}. \quad (35)$$

Since quasi-deuterons are bosons, they can exist only as a condensate in the zero temperature case we are focusing on. For the deuteron there is no thermal contribution to the density but the condensate term

$$n_d^{(v)} = n_d^{(s)} = n_d^{(\text{cond})} \quad (36)$$

with equal vector and scalar densities and the effective chemical potential becomes

$$\mu_d^* = m_d^*. \quad (37)$$

In nuclear matter at very low densities, it is advantageous to form quasi-deuterons, which still have a positive binding energy, to gain energy as compared to a system composed of neutrons and protons only. In SNM, all protons and neutrons will be bound in quasi-deuterons in the low-density limit and no free nucleons remain. The binding energy per nucleon will approach half of the deuteron binding energy for $n_b \rightarrow 0$ and not zero as for homogeneous nucleonic matter without clusters. For ANM, only quasi-deuterons and neutrons (protons) will be the active constituents in case of positive (negative) isospin asymmetry β .

With the help of the nucleon and deuteron densities, a simple expression for the pressure P is found. Since the momentum integral (4) can be calculated explicitly after partial integration, one obtains

$$P = \sum_{q=n,p} \frac{1}{4} \left(\mu_q^* n_q^{(v)} - m_q^* n_q^{(s)} \right) + \frac{1}{2} \left(D_\omega n_\omega^2 + D_\rho n_\rho^2 - D_\sigma n_\sigma^2 \right) + \sum_{i=n,p,d} n_i^{(v)} W_i^{(r)} \quad (38)$$

with

$$D_i = C_i + C'_i n_b \quad (39)$$

for the meson couplings ($i = \sigma, \omega$, and ρ). Because the entropy density (32) vanishes for $T = 0$, the internal energy density \mathcal{E} is identical to the free energy density (31).

2.3 Coupling strength scaling factors

In Eqs. (9)–(13), the scaling factors χ_{ij} appear. These factors are always unitary for nucleons and, in particular,

$$\begin{aligned} \chi_{n\sigma} &= \chi_{n\omega} = \chi_{n\rho} = 1 \\ \chi_{p\sigma} &= \chi_{p\omega} = -\chi_{p\rho} = 1 \end{aligned} \quad (40)$$

for the three mesons. For the nucleons bound in clusters, the choice of the scaling factors is instead widely debated [68].

It is a natural choice to assume that the nucleons inside the deuteron couple to the mesons with the same strength as the unbound nucleons. Nevertheless, previous studies have already shown that, to take into account in-medium effects in calculation of the EoS for astrophysical applications, a universal scaling factor smaller than 1 should be assumed for the cluster-meson coupling strength [69, 70]. A reduced value for the coupling of the σ -meson to different light clusters, including deuterons, allows also a good description of the chemical equilibrium constants determined from the NIMROD data [71]. However, recent Bayesian analysis [72, 73] have highlighted that a larger value should be taken for the cluster σ -meson coupling, to describe recent results from INDRA collaboration as well [74]. Moreover, a possible model-dependence of this result was recently assessed [75], calling for further microscopic analysis to get more stringent constraints. On the other hand, the possible choice of different values for the σ and ω coupling strength factors is known to produce a strong imbalance between the corresponding scalar and the vector potentials. This would, in turn, reflect itself in an unrealistic behavior of the nuclear EoS, owing to a corresponding change of the central potential given by the difference $V_i - S_i$ of very large potentials in lowest order non-relativistic approximation. A reasonable choice would be therefore to assume the same scaling factor for both σ and ω meson ($\chi_{d\sigma} = \chi_{d\omega} = \chi$) and explore the sensitivity of our results to this ingredient ($\chi_{d\rho} = 0$ because the deuteron has zero isospin.) This is thus the strategy that will be adopted in the following.

3 Quasi-deuteron mass shift constraints

In the GRDF, a mass shift Δm_d is introduced in the effective mass defined in Eq. (8) in order to suppress the cluster formation at supra-saturation densities. This mass shift

may generally receive several contributions. For example, in compact star matter, where electrons are included to fulfill the requirement of charge neutrality, a possible contribution comes from the screening of the Coulomb potential produced by the electronic background.

In the nuclear matter case, the mass shift is usually provided just from Pauli blocking, which plays a crucial role in suppressing the cluster formation. Indeed, the Pauli exclusion principle implies that a single-particle state in momentum space would not be longer available for formation of a cluster when it is already occupied by nucleons of the medium. The Pauli blocking of states strongly reduces at high temperatures with increasing diffuseness of the Fermi sphere or when the c.m. momentum of the cluster is much larger than the typical radius of the Fermi sphere. This effect can be represented effectively as a repulsive, medium-dependent potential or a change of the cluster binding energy. A quantitative value can be calculated by solving the many-body Schrödinger equation when proper potentials for the nucleons in matter are introduced. The corresponding results, which are explicitly calculated for various conditions of temperature, density and isospin asymmetry of the medium, are then usually approximated by suitable parameterizations in a wide range of thermodynamic variables [30, 76–78].

The change of the cluster binding energy, calculated in this approach, is valid only at sub-saturation densities and has to be extrapolated to higher densities, in particular above the cluster dissociation (Mott) density, where the binding energy vanishes, and only a many-body correlation in the continuum remains. For this purpose, suitable heuristic parameterizations were introduced within the GRDF [66, 79]. Focusing on deuteron-like correlations, the aim of our work is to provide a unified parameterization of the quasi-deuteron binding energy shifts, so that it can be used as effective means to treat SRCs at supra-saturation densities. In this context, the pioneering analysis developed in Ref. [37] already suggests that a substantial modification of the cluster mass shift has to be expected in the regime beyond the deuteron dissociation density, in comparison to the traditionally adopted form.

Such a parameterization should be appropriately chosen to interpolate between the low-density limit constrained by microscopic many-body calculations and the high-density behavior postulated under the assumed boson condensation condition. In the following subsections the different constraints to be imposed to the deuteron binding-energy shifts will be discussed. As will be seen, various scenarios will emerge depending also on the value of the deuteron-meson scaling factors $\chi = \chi_{d\sigma} = \chi_{d\omega}$ introduced in Eqs. (9)–(13).

3.1 Low-density constraint

Several parameterizations of the binding energy or mass shift of the deuteron at sub-saturation densities have been devel-

oped to account for the Pauli blocking effects. In particular, when neglecting the dependence of the mass shift on the momentum of the deuteron with respect to the medium and limiting to the zero temperature case, the simplified functional form

$$\Delta m_d^{(\text{low})} = \delta B_d(0) n_d^{(\text{eff})} \quad (41)$$

can be assumed, where the effective vector density $n_d^{(\text{eff})}$, as defined in Ref. [37]

$$n_d^{(\text{eff})} = \frac{2}{A_d} \left[N_d \left(n_n^{(v)} + n_d^{(v)} \right) + Z_d \left(n_p^{(v)} + n_d^{(v)} \right) \right] \quad (42)$$

with $N_d = Z_d = 1$ and $A_d = 2$, turns out to be equal to the total baryon density n_b , independent of the global isospin asymmetry β of the system. The quantity δB_d generally regulates the temperature dependence; its zero temperature limit which appears in Eq. (41) is $\delta B_d(0) = 3634.16 \text{ MeV fm}^3$, as given in Ref. [30], where explicit expressions for finite temperature calculations are also provided.

A linear increase of the mass shift proportional to n_b at low baryon densities is consistent with the results obtained in [30, 76–78], at least for density values lying below the dissociation or Mott density defined as

$$n_d^{(\text{diss})} = \frac{B_d}{\delta B_d(0)}, \quad (43)$$

where $B_d = m_n + m_p - m_d = 2.225 \text{ MeV}$ [80] is the deuteron binding energy in vacuum.

3.2 High-density limit

In the traditional treatment of cluster dissolution using the concept of mass shifts, a heuristic density dependence stronger than linear in n_b is customarily assumed at baryon densities above the dissociation density to prevent the clusters to reappear. A divergence of the mass shift ensures in particular the deuteron removal from the system when approaching saturation density, resulting in pure nucleonic matter above saturation. The possibility of using quasi-deuterons to effectively embed nuclear SRCs at supra-saturation densities requires thus a proper change of the usual parameterization adopted in the GRDF, as first noticed in Ref. [37].

3.2.1 Deuteron mass shift

Assuming a dependence on the effective density $n_d^{(\text{eff})} = n_b$, as defined in Eq. (42), the quasi-deuteron mass shift expression derived in Eq. (29) simplifies to

$$\Delta m_d^{(\text{high})} = \mu_n^* + \mu_p^* - m_d + 2\chi C_\sigma n_\sigma + 2(1 - \chi) C_\omega n_\omega \quad (44)$$

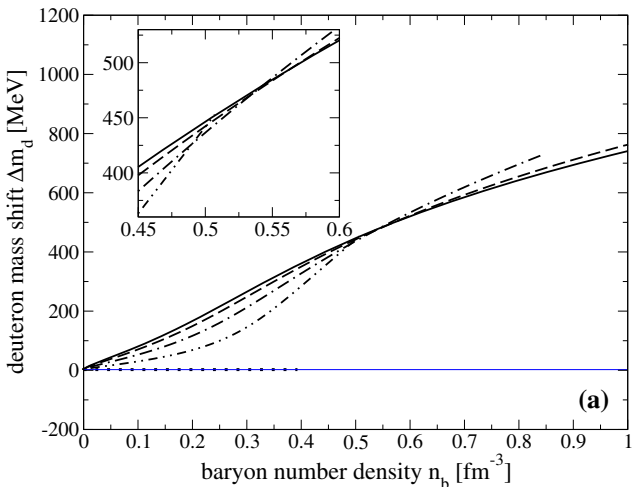
because

$$W_n^{(r)} + W_p^{(r)} - W_d^{(r)} = n_d^{(s)} \frac{\partial \Delta m_d}{\partial n_b} (1 + 1 - 2) = 0. \quad (45)$$

Eq. (44) can be used to calculate the deuteron mass shift as a function of the baryon density n_b , the deuteron fraction X_d and the isospin asymmetry β .

An impression of the density dependence of the quasi-deuteron mass shift is depicted in Fig. 1 for given, constant mass fractions X_d and two values of the scaling factor χ of the deuteron. A unitary value of χ is considered in panel (a), whereas a reduced scaling factor of $\chi = 1/\sqrt{2}$ is assumed in panel (b). The choice of the latter χ value will be explained below. In both panels, for sake of simplicity, the SNM case is considered. Moreover, the DD2 parameterization [30] of the nucleon-meson effective interaction is adopted.

Figure 1 shows that the deuteron mass shift Δm_d depends quite strongly on the value assumed for the scaling factor χ . This is deduced by comparing the results of panel (a) with the corresponding ones of panel (b), especially in the high-density regime, we are focusing on. Indeed, for large densities, the effective chemical potentials of the nucleons in Eq. (44) are dominated by the Fermi momenta k_q as defined in Eq. (33) and thus exhibit a $n_b^{1/3}$ behavior. Since the meson couplings C_σ and C_ω approach constants at high densities, the mesonic contributions to the mass shift are determined by the behavior of the source densities n_σ and n_ω . For $\chi \neq 1$, the source density n_ω rules the dominating term. Since the deuteron fraction has to vanish for $n_b \rightarrow \infty$ due the constraint (27), a linear asymptotic increase of Δm_d with the baryon density is expected. Indeed, such a dependence is



(a)

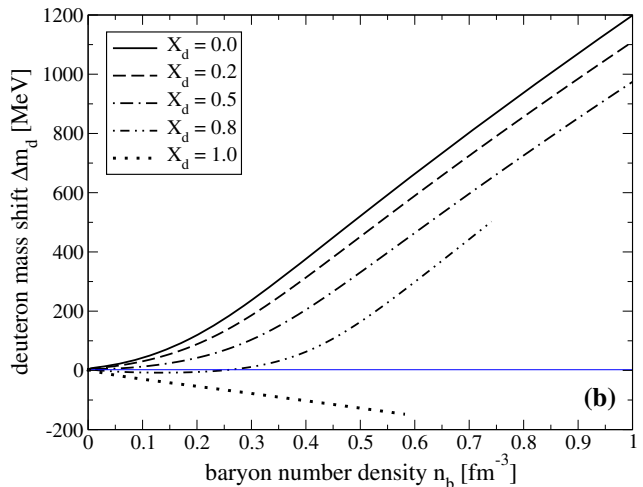
observed in panel (b) of Fig. 1 for $\chi = 1/\sqrt{2}$. A softer increase of the mass shift with the baryon density is seen in panel (a) because the last term in Eq. (44) does not contribute for $\chi = 1$ and the high-density behavior is driven by the σ meson term. However, the source density n_σ may asymptotically receive contributions only from the scalar densities of the nucleons because the deuteron fraction asymptotically approaches zero. An asymptotic dependence proportional to $n_b^{2/3}$ is then expected for the σ meson term and the deuteron mass shift of Eq. (44).

In the (unrealistic) case when all nucleons are bound inside the deuteron ($X_d = 1$), independent of the density, both the scalar and vector densities of the nucleons vanish. The mass shift defined in Eq. (44) assumes the following form

$$\Delta m_d^{(\text{high})}(X_d = 1) = B_d(0) + 2\chi(1 - \chi)(C_\omega - C_\sigma)n_b, \quad (46)$$

i.e., a linear dependence on n_b is generally predicted, for any finite value of the scaling factor χ , as shown by the dotted line of panel (b). An exception is the case with $\chi = 1$, when the deuteron mass-shift coincides with the deuteron binding energy, see dotted line in panel (a).

Furthermore, Fig. 1 shows that the largest deuteron fraction generally corresponds to the lowest mass shift, with a clear ordering in panel (b). However, in the case when a unitary scaling factor is adopted, such a statement actually holds only below the region where the lines cross each other, which is observed above 0.45 fm^{-3} . This region is also emphasized in the inset of panel (a) of Fig. 1 to evidence the fact that there is no single crossing point between the different curves.



(b)

Fig. 1 Panel (a): Deuteron mass shift as function of the baryon density, as determined according to Eq. (44) in the SNM case, by assuming a unitary scaling factor χ for the deuteron-meson coupling strengths. Panel (b): the same as in panel (a), but assuming a reduced scaling factor $\chi = 1/\sqrt{2}$. In both panels, the DD2 parameterization [30] of the

nucleon-meson effective interaction is adopted. The inset in panel (a) shows a zoom around the density values where the curves cross each other. The thin blue line indicates in both panels the binding energy of the deuteron in vacuum B_d

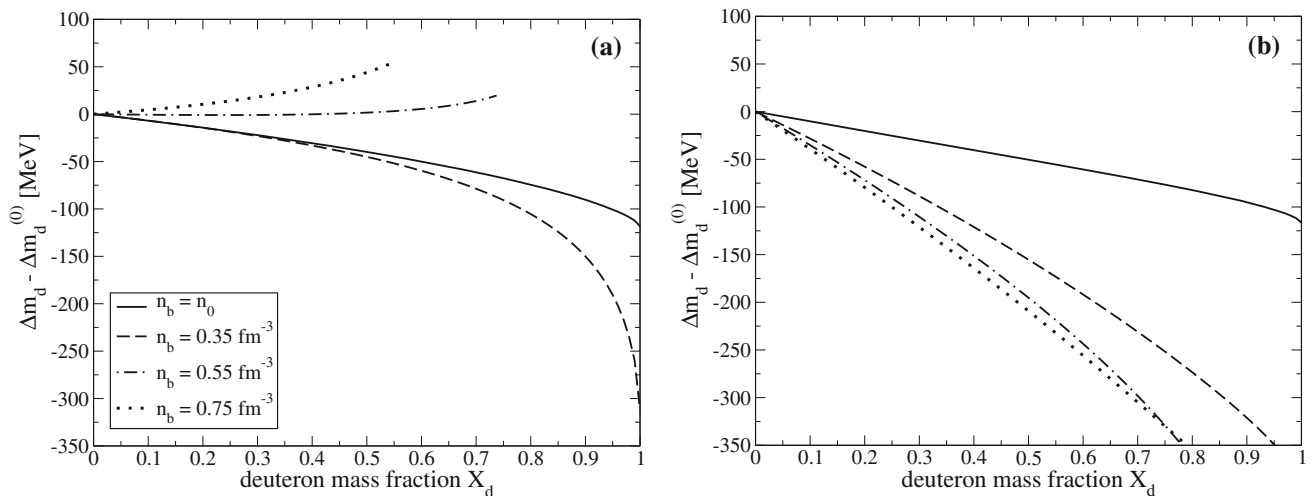


Fig. 2 Panel (a): difference between the deuteron mass shift Δm_d , as determined according to Eq. (44) and its value in the case with zero deuteron mass fraction $\Delta m_d^{(0)}$, as function of the deuteron mass fraction X_d for different, but constant, values of the baryon number density

The emergence of this crossing can be easily understood when looking at the explicit form of Eq. (44). Indeed, for $\chi = 1$, the vector contribution vanishes, and there exists a delicate interplay between the remaining terms. At low densities, the leading role is played by the effective chemical potentials, which reduce when the deuteron mass fraction increases. However, at larger densities, the importance of the term involving the source density of the scalar meson is enhanced. Since the corresponding contribution increases with the deuteron fraction, a crossing among the curves is observed at a certain baryon density n_b^{cross} and an inversion of their previous ordering is expected at higher densities. On the other hand, for smaller values of the scaling factor, as the one considered in panel (b) of Fig. 1, the vector term plays also a role. The source density of the ω meson field does not change with the deuteron mass fraction at constant n_b . Since the vector term dominates asymptotically over the scalar one, in light of the power of density involved there, for scaling factor values small enough, such as the one considered in panel (b) of Fig. 1, no crossing is observed and the same ordering for all allowed densities is preserved.

Moreover, it is worthwhile to notice in panel (a) that the dotted-dashed line, which corresponds to the deuteron mass shift obtained for a fixed deuteron mass fraction $X_d = 0.5$, ends at a density around 0.84 fm^{-3} . Beyond this value, the deuteron mass fraction would exceed its maximum allowed value, see Eq. (27). The same occurs also for the two largest deuteron mass fraction values considered in both panels of Fig. 1, although at smaller densities. It is also worth noticing that Eq. (27) implies that any finite asymptotic value for the deuteron mass fraction is not allowed. As a result, the cluster

n_b . The SNM case is considered and a unitary scaling factor χ for the deuteron-meson coupling strengths are assumed. Panel (b): the same as in panel (a), but assuming a reduced scaling factor $\chi = 1/\sqrt{2}$. In both panels, the DD2 parameterization [30] of the nucleon-meson effective interaction is adopted

is forced to dissolve asymptotically, at least as n_b^{-1} , for any finite value of χ .

The observation of the line crossing in panel (a) of Fig. 1 motivates to study the dependence of the deuteron mass shift on the deuteron mass fraction for constant baryon density n_b and constant asymmetry β . A deeper insight into this behavior can be achieved, by looking at Fig. 2, where Δm_d is plotted as a function of the deuteron mass fraction for different baryon density values. In order to facilitate the comparison among the curves, in Fig. 2 the differences with respect to the deuteron mass shift evaluated in the limiting case without deuteron (denoted as $\Delta m_d^{(0)}$) are actually considered. These differences turn out to be systematically lower than zero, at least for the reduced value of the scaling factor considered in panel (b). A change of sign is instead observed for $\chi = 1$ at larger densities, *i.e.*, beyond the crossing point observed in the panel (a) of Fig. 1 and already discussed above. Quite interestingly, one observes in both panels that the (negative) slope of the curves strongly increases for those lines that approach $X_d = 1$. This represents the ideal, but unrealistic, case where no free nucleons exist in the system also at supersaturation densities. The reason behind this behavior will be clarified in the following, when the mass shift derivatives are investigated in detail.

3.2.2 Mass shift derivatives

In Appendix A, an explicit, general expression for the mass fraction derivative of the mass shift is derived. For sake of simplicity, the case of SNM is considered here, where the Fermi momenta, effective masses and effective chemical potentials of the nucleons are identical, *i.e.*, $k_{\text{nuc}} = k_n = k_p$,

$m_{\text{nuc}}^* = m_n^* = m_p^*$, $\mu_{\text{nuc}}^* = \mu_n^* = \mu_p^*$. Then the simple form

$$\begin{aligned} \frac{\partial \Delta m_d^{(\text{high})}}{\partial X_d} \Big|_{n_b, \beta=0} &= \left[\frac{2C_\sigma}{1 + f_{\text{nuc}} C_\sigma} \left(\chi - \frac{m_{\text{nuc}}^*}{\mu_{\text{nuc}}^*} \right)^2 - \frac{\pi^2}{k_{\text{nuc}}} \frac{1}{\mu_{\text{nuc}}^*} \right] n_b \quad (47) \end{aligned}$$

with the factor

$$f_{\text{nuc}} = 3 \left(\frac{n_{\text{nuc}}^{(s)}}{m_{\text{nuc}}^*} - \frac{n_{\text{nuc}}^{(v)}}{\mu_{\text{nuc}}^*} \right) \quad (48)$$

and the total nucleon densities $n_{\text{nuc}}^{(v)} = n_n^{(v)} + n_p^{(v)}$ and $n_{\text{nuc}}^{(s)} = n_n^{(s)} + n_p^{(s)}$ is obtained. The derivative (47) is the difference of two positive contributions and depending on the choice of χ there can be a zero at a certain baryon density.

The dependence of the derivative (47) on the baryon density n_b is depicted in Fig. 3 panel (a) for $\chi = 1$ and in panel (b) for $\chi = 1/\sqrt{2}$. The same constant values of X_d as in Fig. 1 are considered. Only the limit case with $X_d = 1$ is not shown because for this deuteron mass fraction, k_{nuc} vanishes and a (negative) divergent mass shift derivative is obtained. Moreover, as already observed in Fig. 2, this result is independent of the adopted value for the scaling factor.

Even though we are interested here in the investigation of the high-density limit, it is instructive to study both the low- and high-density behaviors of the derivative (47). One observes that, for $k_{\text{nuc}} \rightarrow 0$, the derivative is dominated by the negative, diverging contribution inside the brackets and the derivative approaches thus zero from negative values, as shown in both panels of Fig. 3. For $k_{\text{nuc}} \rightarrow$

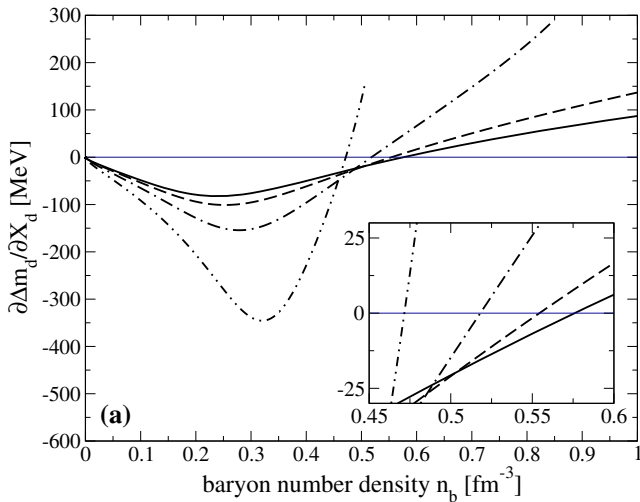


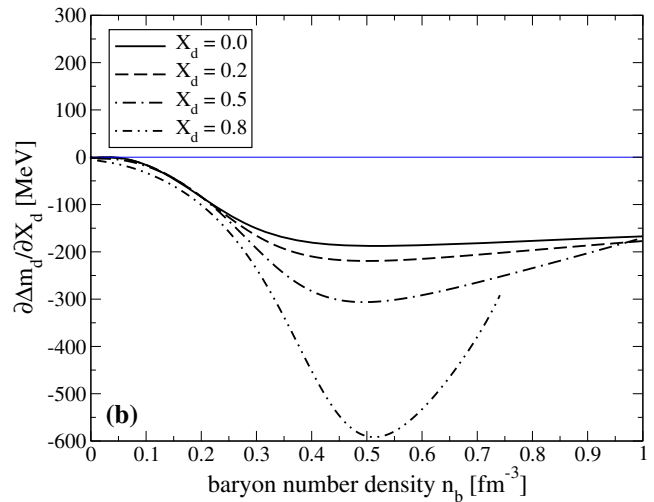
Fig. 3 Panel (a): mass fraction derivative of the deuteron mass shift as function of the baryon density, as determined according to Eq. (47) for different, but constant values of the deuteron mass fraction X_d . The SNM case is considered and a unitary scaling factor χ for the deuteron-meson coupling strengths is assumed. Panel (b): the same as in panel

∞ , the total nucleonic vector and scalar densities scale as $n_{\text{nuc}}^{(v)} \sim [2/(3\pi^2)]k_{\text{nuc}}^3$ and $n_{\text{nuc}}^{(s)} \sim (1/\pi^2)m_{\text{nuc}}^*k_{\text{nuc}}^2$, respectively. Furthermore, $n_b \sim n_{\text{nuc}}^{(v)}$, $m_{\text{nuc}}^* \sim \pi^2/(C_\sigma k_{\text{nuc}}^2)$, and $\mu_{\text{nuc}}^* \sim k_{\text{nuc}}$, so that $f_{\text{nuc}} \sim k_{\text{nuc}}^2/\pi^2$ and the simple asymptotic form

$$\frac{\partial \Delta m_d^{(\text{high})}}{\partial X_d} \Big|_{n_b, \beta=0} \sim (2\chi^2 - 1) \frac{2}{3} k_{\text{nuc}} \quad (49)$$

remains. For $\chi < 1/\sqrt{2}$ the derivative in the high-density limit is negative as for $k_{\text{nuc}} \rightarrow 0$ and no zero at finite baryon densities is expected. In contrast, for $\chi = 1$, the derivative approaches asymptotically a positive value and a zero at a certain baryon value, n_b^{cross} , appears, as depicted in Fig. 3, panel (a). The curves cross the zero line at similar values above 0.45 fm^{-3} with a weak dependence on the deuteron fraction, highlighted in the inset. Below the crossing an ordering of the lines as observed in panel (b) of Fig. 1 follows, whereas an inversion will appear above n_b^{cross} . For $\chi = 1/\sqrt{2}$, however, the derivative of the mass shift with respect to the deuteron mass fraction of Eq. (47) is always non-positive, as evidenced in the panel (b) of Fig. 3. Then, the zero line is only asymptotically approached and $\chi = 1/\sqrt{2}$ constitutes the largest value for which the ordering of the lines with respect to X_d , depicted in Fig. 1, panel (b) persists, for all baryon densities.

In the following, also the derivative of the mass shift with respect to the baryon density will be studied. It can be calculated explicitly from Eq. (44). The general case for arbitrary values of β is treated in Appendix B. Again, the result for the simplified case of SNM is given here. It can be written



(a), but assuming a reduced scaling factor $\chi = 1/\sqrt{2}$. In both panels, the DD2 parameterization [30] of the nucleon-meson effective interaction is adopted. The thin blue line indicates the zero of the deuteron mass fraction derivative of the mass shift. The inset in panel (a) shows a zoom around the density where the derivative vanishes

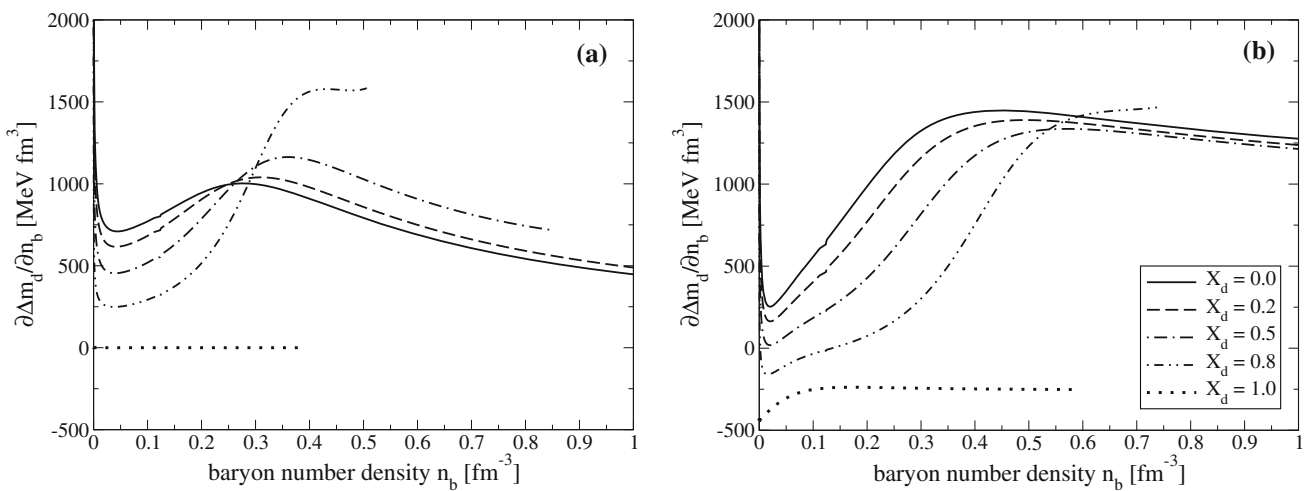


Fig. 4 Panel (a): Baryon density derivative of the deuteron mass shift as function of the baryon density, as determined according to Eq. (50) for different, but constant values of the deuteron mass fraction X_d . The SNM case is considered and a unitary scaling factor χ for the deuteron-

meson coupling strengths is assumed. Panel (b): the same as in panel (a), but assuming a reduced scaling factor $\chi = 1/\sqrt{2}$. In both panels, the DD2 parameterization [30] of the nucleon-meson effective interaction is adopted

for $\chi = \chi_{d\omega} = \chi_{d\sigma}$ as

$$\frac{\partial \Delta m_d^{(\text{high})}}{\partial n_b} \Big|_{\beta=0} = \mathcal{W}_d^{\text{SNM}} - \mathcal{Z}_d^{\text{SNM}} \frac{\partial (n_b X_d)}{\partial n_b} \Big|_{\beta=0} \quad (50)$$

with the quantities

$$\begin{aligned} \mathcal{Z}_d^{\text{SNM}} = & \frac{\pi^2}{\mu_{\text{nuc}}^* k_{\text{nuc}}} + 2(1-\chi)^2 C_\omega \\ & - \frac{2C_\sigma}{1+f_{\text{nuc}} C_\sigma} \left(\chi - \frac{m_{\text{nuc}}^*}{\mu_{\text{nuc}}^*} \right)^2 \end{aligned} \quad (51)$$

and

$$\begin{aligned} \mathcal{W}_d^{\text{SNM}} = & \frac{\pi^2}{\mu_{\text{nuc}}^* k_{\text{nuc}}} + 2(1-\chi) (C_\omega + C'_\omega n_\omega) \\ & + \frac{2}{1+f_{\text{nuc}} C_\sigma} \left(C'_\sigma n_\sigma + C_\sigma \frac{m_{\text{nuc}}^*}{\mu_{\text{nuc}}^*} \right) \left(\chi - \frac{m_{\text{nuc}}^*}{\mu_{\text{nuc}}^*} \right) \end{aligned} \quad (52)$$

that contain again the factor (48). The dependence of the derivative (50) for the SNM case is depicted in the two panels of Fig. 4 for the selected scaling factors of $\chi = 1$ (left) and $\chi = 1/\sqrt{2}$ (right). In the zero-density limit, a divergent behavior is observed, owing to the contribution originating from the density derivatives of the effective chemical potentials that lead to the terms proportional to k_{nuc}^{-1} in $\mathcal{Z}_d^{\text{SNM}}$ and $\mathcal{W}_d^{\text{SNM}}$. The divergence of (50) for $n_b \rightarrow 0$ will disappear only for constant $X_d = 1$. The relative importance of the terms proportional to k_{nuc}^{-1} strongly reduces with increasing density, so that a rise driven by the σ meson contribution is observed at larger n_b values, until a maximum is reached. Then, a continuous decrease of the density derivative of the deuteron mass shift emerges, which asymptotically

approaches zero or a constant value for the unitary or the reduced value of χ , respectively. An interplay among the different involved terms takes place, analogously to the one illustrated to describe the results of Fig. 1. As a consequence, the ordering of the curves in Fig. 1 is reflected in Fig. 4. As discussed before, for any finite deuteron fraction value X_d , the corresponding curve ends again at the baryon density where $X_d^{(\text{max})}$, as a function of n_b , attains this value.

4 Mass shift parameterization

The condensation condition allows to calculate, for a given mass-fraction function, the quasi-deuteron mass shift and its derivatives at high-densities through Eqs. (44), (47) and (50), respectively. However, the density dependence of the mass fraction X_d is not known a priori, in particular at supra-saturation densities. It should originate from microscopic calculations in a similar manner as the fractions of light clusters are determined by their mass shifts in the low-density domain, see Ref. [30]. Since calculations of the deuteron mass shift using proper interactions and many-body methods are only available at very low densities, it is necessary to resort to exemplary forms of the mass shift in the full range of baryon densities to study the properties of the system. Instead of calculating the mass shift and its derivatives for a given mass fraction function, the main aim is then to choose a density dependent parameterization of the mass shift and to determine the deuteron fraction, not only for symmetric but also asymmetric matter. Although such a function is not yet available from microscopic models, the proposed form should comply with the available constraints.

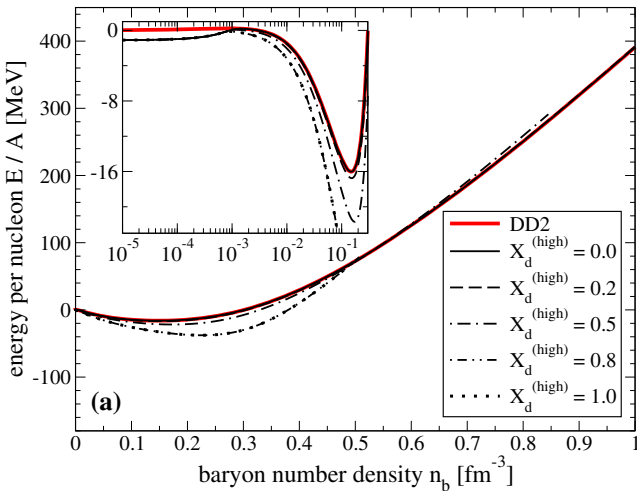
4.1 Piecewise mass-shift parameterization

The most simple choice for the deuteron mass shift function is the piecewise parameterization

$$\Delta m_d(n_b) = \min \left\{ \Delta m_d^{(\text{low})}(n_b), \Delta m_d^{(\text{high})}(n_b, X_d) \right\} \quad (53)$$

that combines the low-density form (41) with the high-density function (44) assuming, e.g., a constant deuteron fraction in the high-density region as discussed in the previous subsection. Although Eq. (53) provides a continuous function, the same does not apply for its derivatives. In addition, a constant deuteron fraction at high densities is not compatible with the asymptotic constraint which imposes a vanishing mass fraction X_d for $n_b \rightarrow \infty$.

Despite these shortcomings, it is informative to investigate the effect of finite deuteron fractions on the energy per nucleon E/A . Fig. 5 depicts the density behavior of E/A in SNM as obtained with the piecewise mass shift parameterization (53) for different, but constant mass fractions in the high-density regime. For comparison, the energy per nucleon obtained from the deuteron free case of the standard DD2 parameterization is also shown. One observes that an extra binding is predicted in the energy per nucleon around saturation density, with respect to the case without deuterons. This result is independent of the adopted choice of the scaling factor χ of the deuteron-meson couplings. Moreover, Fig. 5 shows that the overbinding persists much beyond the saturation density, especially in panel (b), where a reduced value of χ is considered. However, the stiffness of these curves in the high-density regime increases with the deuteron mass



fraction. As a result, a crossing among the curves is generally observed at larger densities in case when $\chi \geq 1/\sqrt{2}$, except for deuteron fraction values for which the corresponding curves end at lower densities.

Both insets of Fig. 5 highlight that the correct low-density limit is reproduced because the low-density constraint is properly taken into account. As a result, differently from the standard DD2 model without clusters, the curves tend to half the deuteron binding energy in the limit $n_b \rightarrow 0$.

The overbinding observed in Fig. 5 in a broad range of densities around saturation seems to be surprising in light of the large positive mass shift of the deuteron depicted in Fig. 1. The increase of the binding energy per nucleon is a result of two main effects. When nucleons are replaced by quasi-deuterons at a given baryon density, the value of n_ω does not change when $\chi = 1$. At the same time, the source density n_σ increases because the scalar and vector densities of the condensed deuterons are identical whereas $n_q^{(s)}/n_q^{(v)} < 1$ for nucleons. Hence, on the one hand, a stronger attraction from the σ meson is induced. This effect will be smaller for $\chi < 1$ when nucleons are replaced by deuterons. Here, the source density of the ω meson will reduce but the corresponding decrease of the σ meson source density is also less strong. On the other hand, nucleons at the Fermi surface with energies close to the nucleon chemical potential

$$\mu_q^{(0)} = \sqrt{\left(k_q^{(0)}\right)^2 + \left(m_q - S_q^{(0)}\right)^2} + V_q^{(0)} \quad (54)$$

of the deuteron-free system, indicated by a superscript (0), are replaced by deuterons with energy

$$E_d = \mu_d = m_d - S_d + V_d + \Delta m_d = \mu_n + \mu_p. \quad (55)$$

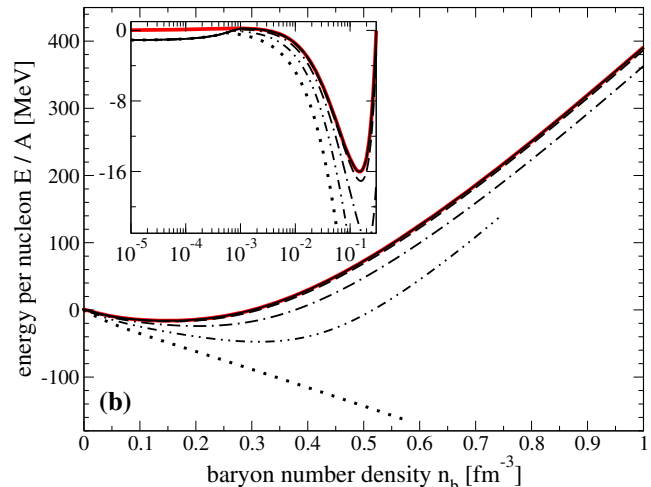


Fig. 5 Panel (a): energy per nucleon as function of the baryon density as determined in the SNM case, by assuming a unitary scaling factor χ for the deuteron-meson coupling strengths. A simple piecewise parameterization, as given by Eq. (53) and interpolating between the low- and high-density constraints for the mass shift is adopted. Different, but con-

stant, values of the deuteron mass fraction $X_d^{(\text{high})}$ at high density are considered. Panel (b): the same as in panel (a), but assuming a reduced scaling factor $\chi = 1/\sqrt{2}$. In both panels, the DD2 parameterization [30] of the nucleon-meson effective interaction is adopted

Since $k_q < k_q^{(0)}$, $S_q > S_q^{(0)}$, and $V_q \approx V_q^{(0)}$, the chemical potentials of the nucleons μ_q are lowered, i.e., $\mu_q < \mu_q^{(0)}$, even for a positive deuteron mass shift Δm_d . This corresponds to a stronger binding of the system.

4.2 Specific features in the determination of deuteron mass fractions from mass shifts

In principle, it would be sufficient to use the condensation condition (44) to find X_d for a given $\Delta m_d^{(\text{high})}$. In practice, however, it is found that, in the high-density regime, Eq. (44) can have multiple solutions when a meson coupling scaling factor $\chi \geq 1/\sqrt{2}$ is considered. As a consequence, Eq. (44) can not be inverted uniquely in all cases. The correct solution has to be selected such that a continuous function of the density is obtained for the deuteron mass fraction.

In this context, further insight can be obtained from the explicit functional form of the mass shift derivative with respect to the density, given by Eq. (50). It is, in fact, a first-order differential equation for X_d . The expression can be analyzed most easily for SNM. It is convenient to write Eq. (50) in the form

$$\frac{\partial(n_b X_d)}{\partial n_b} \Big|_{\beta=0} = \frac{1}{\mathcal{Z}_d^{\text{SNM}}} \left(\mathcal{W}_d^{\text{SNM}} - \frac{\partial \Delta m_d}{\partial n_b} \Big|_{\beta=0} \right) \quad (56)$$

with the functions $\mathcal{Z}_d^{\text{SNM}}$ and $\mathcal{W}_d^{\text{SNM}}$ as defined in Eqs. (51) and (52), respectively. A special role is played by $\mathcal{Z}_d^{\text{SNM}}$ that can be written as

$$\mathcal{Z}_d^{\text{SNM}} = 2(1-\chi)^2 C_\omega - \frac{1}{n_b} \frac{\partial \Delta m_d}{\partial X_d} \Big|_{n_b, \beta=0} \quad (57)$$

with the help of the mass fraction derivative defined in Eq. (47). The superscript (high) is no longer added to the mass shift because a mass shift parameterization is considered now in the whole density range. For $\chi = 1$, the term from the ω meson does not contribute. The remaining term in Eq. (57) develops a zero at a certain density n_b^{cross} as discussed in Sect. 3.2 close to Eq. (49). Thus the density derivative (56) develops a pole at x_b^{cross} and a continuous solution of the differential equation can only be obtained if the term in parentheses in Eq. (56) vanishes at the same density. For $\chi \leq 1/\sqrt{2}$, however, the mass-fraction derivative (47) is negative, implying a positive $\mathcal{Z}_d^{\text{SNM}}$ because also the contribution of the ω meson is positive. Then, a continuous solution of the differential equation (56) can be found for all densities. The discussion developed above justifies the choice of the reduced scaling factor. Thus, two different values of the scaling factor, namely $\chi = 1$ and $\chi = 1/\sqrt{2}$, will be considered in the following analysis. It is worthwhile to notice that the value of

$\chi = 1/\sqrt{2}$ is significantly smaller than the universal scaling factor for the cluster-meson coupling strength proposed in some recent works [69, 70]. Our choice complies, however, with the aim to consider two extreme values of χ with two distinct paths, bearing in mind that any intermediate behavior may also occur.

4.3 Saturation constraints

The overbinding observed around saturation density in both panels of Fig. 5 implies that a proper refit of the nucleon-meson couplings to the saturation properties of SNM is mandatory if one wants to keep nuclear matter quantities around the saturation point n_0 well constrained. The actual deuteron fraction at saturation, $X_{d,0}$, which has to be specified to fix the couplings, can be imposed from recent experimental investigations of SRCs by extrapolating results of nuclei to infinite nuclear matter. They assess that SRCs pairs amount to approximately 20% of the nucleon density [43–45]. Here, as in the following, the index 0 on the quantities indicates the values at saturation.

In order to reproduce the properties at saturation in SNM, e.g., of the DD2 model, the binding energy per nucleon B_0 and the effective nucleon mass $m_{\text{nuc},0}^*$ at the saturation density should be obtained also in the model with a finite deuteron fraction $X_{d,0}$. This will be realized by rescaling the meson-nucleon couplings assuming no change in their density dependence as given in a reference parameterization. The values of n_0 , B_0 , $m_{\text{nuc},0}$ and $X_{d,0}$ together with the pressure $P_0 = 0 \text{ MeV fm}^{-3}$ give four conditions that allow to determine the rescaled couplings $\Gamma_{\sigma,0}$, $\Gamma_{\omega,0}$, the deuteron mass shift $\Delta m_{d,0}$ and its derivative $d\Delta m_d/dn_b|_{n_0}$ at saturation. Owing to the rescaling of the σ and ω coupling strengths, also the energy per nucleon of PNM would be modified. A proper rescaling also of the ρ -nucleon coupling strength is hence in order if one wants to keep the symmetry energy at saturation J_0 unaltered, with respect to the selected reference parameterization. Here, the symmetry energy is calculated in the parabolic approximation as the difference between the energies per nucleon in PNM and SNM. This recipe gives finite values at sub-saturation densities in models with clusters or liquid-gas phase transition differently than the original definition using second derivatives of the energy per nucleon in SNM with respect to the isospin asymmetry, see, e.g., Ref. [81]. The full conversion procedure is illustrated in detail in Appendix C. The actual values of these quantities are given in Table 1 for the two considered values of the deuteron coupling scaling factor χ and a deuteron fraction $X_{d,0} = 0.2$. The standard DD2 model is chosen as reference parameterization with $n_0 = 0.149065 \text{ fm}^{-3}$, $B_0 = 16.0224 \text{ MeV}$, $m_{\text{nuc},0}^* = 0.562544 m_{\text{nuc}}$ and $J_0 = 32.73 \text{ MeV}$. The σ , ω , and ρ nucleon-meson couplings are given by $\Gamma_{\sigma,0} = 10.686681$, $\Gamma_{\omega,0} = 13.342362$ and $\Gamma_{\rho,0} = 3.626940$ in this case.

Table 1 Values at saturation density of nucleon-meson coupling strengths $\Gamma_{j,0}$ ($j = \sigma, \omega, \rho$), deuteron mass shift $\Delta m_{d,0}$ and its slope, for the two different scaling factors χ considered in this work. The mass

χ	$\Gamma_{\sigma,0}$	$\Gamma_{\omega,0}$	$\Gamma_{\rho,0}$	$\Delta m_{d,0}$ [MeV]	$\left. \frac{d\Delta m_d}{dn} \right _{n_0, \beta=0}$ [MeV fm ³]
1	10.580042	13.217226	3.556424	104.92	813.98
$1/\sqrt{2}$	10.919963	13.719324	3.400187	58.23	570.80

Quite interestingly, one observes that, in the case with a unitary scaling factor χ , a small reduction of the three nucleon-meson coupling strengths is obtained at saturation, with respect to the original DD2 parameterization. On the other hand, these quantities turn out to be larger for both σ - and ω -meson, when the smaller χ value is considered. This change reflects the balance between the couplings and scaling factors to achieve the same strength of the effective interaction at saturation density. Concerning the mass shifts, larger values and stronger density slopes are predicted at saturation when assuming that the nucleons bound inside the deuterons couple to the mesons with the same strength as the unbound nucleons, see also Fig. 1.

A possible mass shift parameterization will be proposed in the following section. It will be constrained at saturation density, in the low-density limit by microscopic many-body calculations and at high-density by an assumed mass-fraction behavior that respects the condensation condition and the constraint on the maximum deuteron fraction.

4.4 Unified mass shift parameterization

Different forms of the mass shift density parameterization might be employed to interpolate among the low- and the high-density constraints discussed in the previous section, while keeping the required saturation properties. A unified form, adopted for the SNM case, might be then employed also for ANM to obtain predictions at arbitrary isospin asymmetries. The mass shift parameterization introduced in this work combines two limiting dependencies on the density that reproduce by construction the linear increase in the zero-density limit of the dilute region and the high-density asymptotic behavior. Taking into account also the two constraints imposed at saturation, such a parameterization has to depend on at least four parameters and satisfy $\Delta m_d(0) = 0$. However, some additional parameters should enter in the proposed parameterization to guarantee a smooth transition between the different density regimes and leave some freedom in the high-density behavior of the deuteron fraction.

A possible choice, among others, is the function

$$\Delta m_d(x) = \Delta m_{d,1}(x) + \Delta m_{d,2}(x) + \Delta m_{d,3}(x) \quad (58)$$

shift and its slope are expressed in MeV and MeV fm³, respectively, whereas all other quantities are dimensionless

χ	$\Gamma_{\sigma,0}$	$\Gamma_{\omega,0}$	$\Gamma_{\rho,0}$	$\Delta m_{d,0}$ [MeV]	$\left. \frac{d\Delta m_d}{dn} \right _{n_0, \beta=0}$ [MeV fm ³]
1	10.580042	13.217226	3.556424	104.92	813.98
$1/\sqrt{2}$	10.919963	13.719324	3.400187	58.23	570.80

depending on $x = n_b/n_0$ with three contributions

$$\Delta m_{d,1}(x) = \frac{ax}{1+bx} \quad (59)$$

$$\Delta m_{d,2}(x) = cx^{\eta+1} [1 - \tanh(ex)] \quad (60)$$

$$\Delta m_{d,3}(x) = fx^\gamma \tanh(gx) \quad (61)$$

with $\gamma = 1$ or $2/3$ for $\chi = 1/\sqrt{2}$ or 1, respectively, and seven coefficients a, b, c, η, e, f, g , which allow to comply with the constraints by a proper choice.

The different terms in Eqs. (58)–(61) are chosen so that the density derivative of the mass shift is given by

$$\left. \frac{d\Delta m_d}{dn_b} \right|_{n_b=0} = \frac{a}{n_0} \quad (62)$$

at vanishing n_b and the high-density behavior is dominated by the third term $\Delta m_{d,3}$. The second contribution acts mainly in an intermediate density range. The coefficient a is determined as $\delta B_d(0)n_0$ by the limiting form of the deuteron mass shift parameterization from microscopic calculations, c.f., Eq. (41). There is no a priori constraint for the parameter b . Here, it is set to $b = a/B_d = n_0/n_d^{(\text{diss})}$ so that $\lim_{n_b \rightarrow \infty} \Delta m_{d,1} = B_d$ with the deuteron binding energy B_d and the dissociation density $n_d^{(\text{diss})}$ defined in Eq. (43). In the asymptotic limit, for $\chi = 1/\sqrt{2}$, the mass shift approaches a linear function in the baryon density and a slope determined by the ratio of f and the saturation density n_0 . On the other hand, the asymptotic form

$$\Delta m_d(n_b) \sim f \left(\frac{n_b}{n_0} \right)^{2/3} \quad (63)$$

is expected for the deuteron mass shift, in the case when $\chi = 1$.

The coefficients c and η , whose analytical expressions are given in Appendix D, are finally determined by the constraints introduced on the mass shift and its derivative at saturation. The remaining parameters e and g are free and allow to tune the relative role of the different contributions $\Delta m_{d,2}$ and $\Delta m_{d,3}$ in Eq. (58). Only a tiny sensitivity of the results was assessed by varying the parameter e . Thus, this parameter was kept fixed to 1 and only different values for the parameter g were considered. Different choices of g permit indeed to

produce alternative supra-saturation scenarios while keeping the same asymptotic behavior.

4.4.1 Deuteron mass shift and mass fraction for $\chi = 1$

Let us consider first the case with $\chi = 1$. For such a scaling factor, three different sets of parameters will be considered. They are determined according to the parameterization proposed in Eqs. (58)–(61) with $\gamma = 2/3$ and are labeled in the following as DD2-d1, DD2-d2 and DD2-d3. The values of the parameters for these mass shift parameterizations are listed in the first three lines of Table 2. They were obtained by employing the DD2 nucleon-meson effective interaction with properly rescaled meson coupling strengths at saturation as given in Table 1. Panel (a) of Fig. 6 shows the deuteron mass

shift as function of the baryon density for these three different sets. The red shaded area corresponds to the range of possible mass shift values that are explored by assuming, for each density, deuteron fractions within the range $[0, \min\{1, X_d^{(\max)}\}]$. First of all, Fig. 6 highlights the validity of the proposed parameterization to comply with the constraints imposed on the deuteron mass-shift. The three lines lie indeed within the red area for the whole range of displayed baryon densities.

However, as shown in Table 2, a rather small range of the parameter g may be actually explored, owing to the shrinkage of the red area in the density region around the crossing points, which were observed in Fig. 1, panel (a). Despite their proximity, when these parameterizations are employed in Eq. (56) to determine the density behavior of the deuteron fraction, extremely different outcomes are obtained, at least when

Table 2 Values of the parameters in the deuteron mass shift parameterization defined by Eqs. (58)–(61) for six different sets. They are obtained by employing the DD2 nucleon-meson effective interaction, with properly rescaled meson coupling strengths at saturation. The parameters a ,

	a	b	c	η	e	f	g	γ
DD2-d1	541.726060	243.472387	-83.230901	3.491787	1.0	214.368137	0.65	2/3
DD2-d2	541.726060	243.472387	-98.923123	3.200967	1.0	214.368137	0.67632	2/3
DD2-d3	541.726060	243.472387	-140.309501	2.715545	1.0	214.368137	0.75	2/3
DD2- χ d1	541.726060	243.472387	99.677247	1.656159	1.0	181.113975	0.18	1
DD2- χ d2	541.726060	243.472387	70.476986	1.230947	1.0	181.113975	0.22	1
DD2- χ d3	541.726060	243.472387	41.777908	0.257252	1.0	181.113975	0.26	1

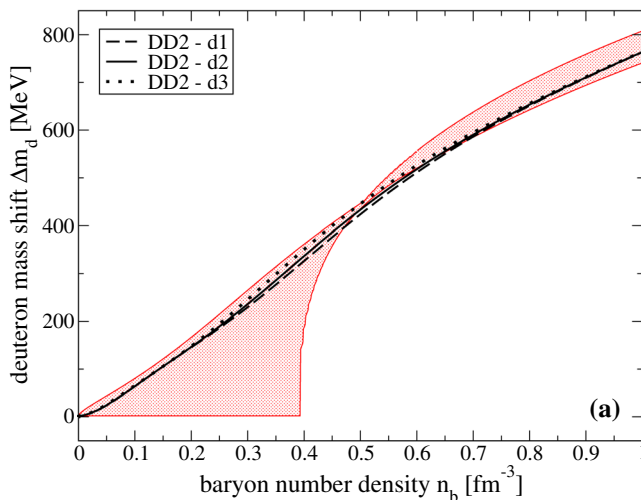
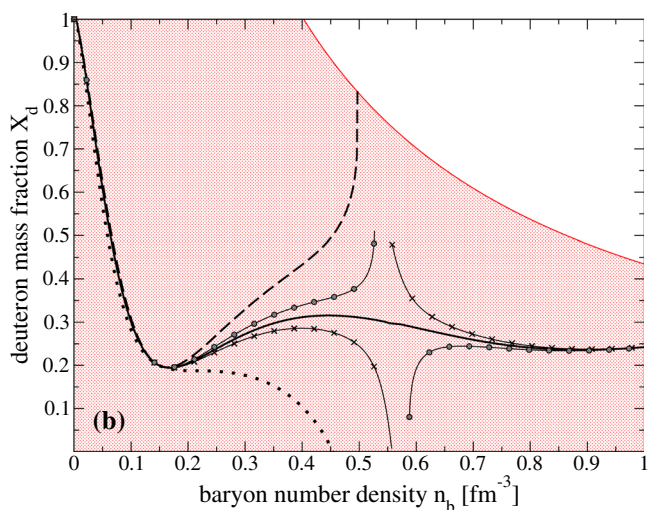


Fig. 6 Panel (a): deuteron mass shift as function of the baryon density, as determined according to the parameterization proposed in Eqs. (58)–(61). The SNM case is considered and a scaling factor $\chi = 1$ is assumed for the deuteron-meson coupling strengths. Three different set of parameters were employed. The red shaded areas evidence the region of allowed mass shift or deuteron mass fraction values. Panel (b): deuteron mass fraction X_d as function of the baryon density, as

c and f are expressed in MeV, b , η , e , g and γ are dimensionless. The first three sets refer to the case with deuteron-meson coupling scaling factor $\chi = 1$, the others to $\chi = 1/\sqrt{2}$



determined by employing the same sets of parameters considered in panel (a). In both panels, the DD2 nucleon-meson effective interaction, with properly rescaled meson coupling strengths at saturation, is adopted. Two curves with symbols (not shown in panel (a)) are considered in panel (b), as a result of slightly varying the g parameter of the set labeled as DD2-d2 (see text for more details)

approaching the region of the crossings. As clearly depicted in Fig. 6, panel (b), the three adopted parameterizations correctly reproduce the low-density limit, corresponding to the situation in which the matter is entirely clusterized ($X_d = 1$), and account also for the constraints at saturation.

Nonetheless, highly diverse scenarios are predicted at high-densities. The dashed curve, which is the lowest one in the region around the shrinkage observed in panel (a), corresponds to a deuteron mass fraction which tends to exceed, at a certain density, the maximum allowed value for $X_d^{(\max)}$. We remind that the density region beyond this point would be characterized by a negative value of the Dirac effective mass of the nucleons. To exclude this opportunity, the curve in Fig. 6, panel (b) is thus stopped beyond that density. Owing to the unfeasible high-density scenario, this set of parameter will not be further employed in the following. Conversely, the DD2-d3 parameterization, plotted as the dotted line, lying above the other curves around 0.5 fm^{-3} in panel (a), predicts a sudden disappearance of the deuterons, when approaching the pole of Eq. (56). Actually, even in this case, the curve is not plotted beyond the region of the crossing, to exclude the unrealistic situation in which the clusters reappear at very high densities. As already anticipated in Sect. 4.2, a quasi-continuous solution of Eq. (56) might be arranged for all densities with a fine tuning of the parameters. The corresponding curve is plotted in both panels of Fig. 6 as the full line. In this case, a smooth behavior is apparently recovered for the density behavior of the deuteron mass fraction. However, a strong sensitivity persists in correspondence of the pole, as manifested by the two thin lines with symbols plotted in panel (b). These curves are obtained with mass shifts functions that are found by varying the g parameter only by 1% of the set labeled as DD2-d2. Owing to the presence of the pole, the DD2-d2 set of parameters will be set aside hereafter too. A more refined method to find a continuous function would be to consider a more general form of the mass shift parameterization with respect to the one proposed in Eqs. (58)–(61). By enlarging the number of the involved parameters, it would be possible to constrain the mass-shift and its slope values such that the pole will be definitely washed out. Nonetheless, none of such possible parameterizations would allow to accomplish our aim to extend the predictions to ANM. Since the position of the pole evolves with the asymmetry, a divergence of the mass fraction would emerge once again as soon as the asymmetry of the matter is changed, despite its removal in the SNM case. The same holds, obviously, for any deuteron-meson coupling scaling factor $\chi > 1/\sqrt{2}$. However, one should bear in mind that, for values of the scaling factor smaller than 1, the pole is expected to appear at higher densities. Since for $\chi = 1$ the pole emerges already at rather large densities (around $3n_0$), one expects that for more realistic values of χ , its position will be located much beyond the range that is relevant in the applications of the

model. Then its emergence could be neglected in practice. For $\chi = 1$, only the DD2-d3 parameterization will be employed in the following, when the general properties of both SNM and ANM matter will be investigated.

4.4.2 Deuteron mass shift and mass fraction for $\chi = 1/\sqrt{2}$

As discussed in the previous sections, a possible way out to overcome the issue of the pole might be to assume a smaller scaling factor which is, at maximum, equal to $1/\sqrt{2}$. For such a scaling factor, three different sets of parameters, labeled as DD2- χ d1, DD2- χ d2, and DD2- χ d3, are proposed here. The values of the parameters in Eqs. (58)–(61) for these sets are listed again in Table 2.

One observes a strong sensitivity to the g parameter of the deduced values for c and η . Moreover, when increasing g , both parameters to account for the saturation constraints decrease. A further increase of g beyond a maximum value $g_{\max} \approx 0.26$ is excluded, since it would imply a negative value for d and thus a dominant role of $\Delta m_{d,2}$ in the zero-density limit, where a pole could even emerge. However $\Delta m_{d,1}$ returns already, by construction, the correct low-density trend.

Further insights may be achieved by looking at both panels of Fig. 7. The density behaviors of these mass shifts are shown in Fig. 7 panel (a). The same parameterizations are then employed in panel (b) of Fig. 7 to determine the corresponding density behavior of the deuteron mass fraction X_d . In the two panels, the red shaded area evidences the allowed region between the (upper) curve, related to the deuteron-free case, *i.e.* $X_d = 0$, and the (lower) one, obtained by assuming $X_d = \min \{1, X_d^{(\max)}\}$.

First of all, looking at panel (a), one notices that the black curves lie always within the red shaded area up to very large baryon densities, so validating the choice of the adopted parameter sets. In light of the constraints imposed in the extremely dilute regime and at saturation, the full, dashed and dotted black curves remain rather close up to n_0 . All the curves also converge to the line characterized by $X_d = 0$, in the asymptotic limit. Some differences emerge instead in the high-density behavior, around and beyond $3n_0$.

The observed differences in the mass shifts are then reflected in the density behavior of the deuteron mass fraction, which is plotted in panel (b). Independent on the parameterization, in the zero-density limit, the matter is completely clusterized and the deuteron mass fraction X_d is equal to 1. With increasing density, a considerable reduction of X_d is observed and a local minimum emerges in a density region around the saturation density. There the value $X_d = 0.2$ is reached, as required in agreement with the experimental evidences concerning the emergence of SRCs pairs. At supersaturation densities, several scenarios take place. The curves

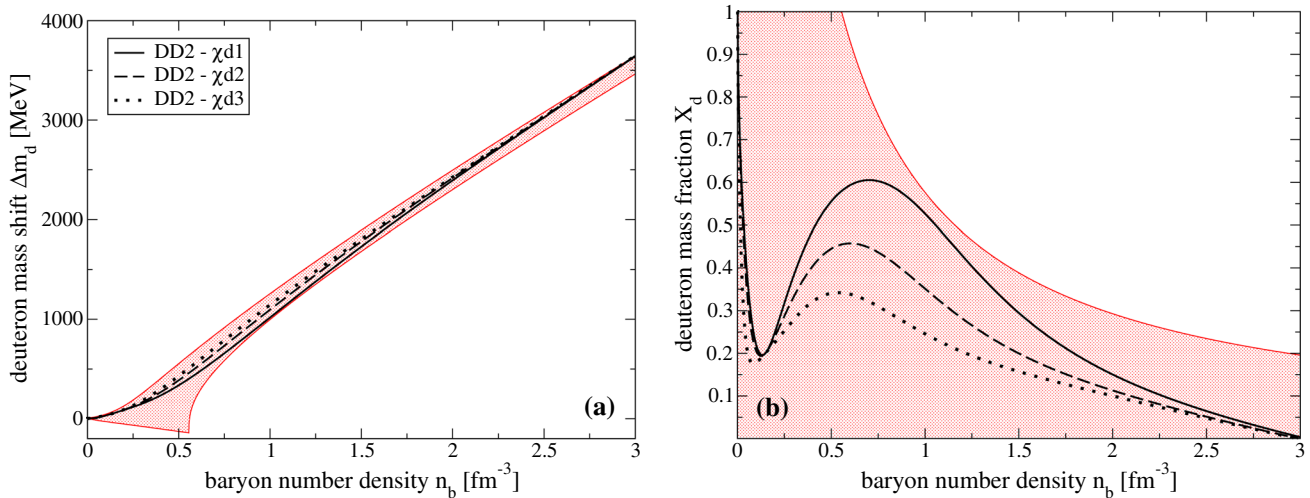


Fig. 7 Panel (a): deuteron mass shift as function of the baryon density, as determined according to the parameterization proposed in Eqs. (58)–(61). The SNM case is considered and a scaling factor $\chi = 1/\sqrt{2}$ is assumed for the deuteron-meson coupling strengths. Three different set of parameters were employed. The red shaded area evidences the region between the (upper) curve, related to the deuteron-free case, *i.e.* $X_d = 0$,

never overshoot the line indicating the maximum allowed value for X_d , which ensures a non-negative value for the Dirac effective mass of the nucleons. Then, at higher densities, a decreasing trend is observed for all curves, which converge each other, approaching zero asymptotically.

It is worthwhile to notice that alternative scenarios, similar to the ones displayed by the dotted and the dashed lines in panel (b) of Fig. 6, would be possible also in the case with $\chi = 1/\sqrt{2}$. Solutions with deuteron mass fraction values which tend to exceed the maximum allowed at a certain density or abruptly vanishing might accidentally occur, when considering mass shift parameterizations which cross the lowest or the highest border, respectively, of the red shaded area shown in panel (a) of Fig. 7. Differently than the case with $\chi = 1$, these solutions are not connected to the emergence of any pole. The three sets of parameters proposed in panel (b) of Fig. 7 avoid these scenarios. Solutions with the disappearance of the clusters at a certain baryon density would be likewise acceptable, even though none of the three chosen sets of parameters for $\chi = 1/\sqrt{2}$ provides a similar result. Indeed, for this class of solutions, the density behavior of the deuteron mass fraction would closely resemble the one obtained with the DD2-d3 parameterization. The main difference will be only the possible wider density range with a non-vanishing deuteron mass fraction values before the cluster is suppressed. For $\chi = 1/\sqrt{2}$, we will consider three set of parameters, such that the mass shifts are characterized by similar smooth trends as functions of the baryon density, but different sizes of the deuteron mass fractions in the supra-saturation density regime. In such a way, we could assess and isolate the role of this ingredient.

and the (lower) one, obtained by assuming $X_d = \min \{1, X_d^{(\max)}\}$. Panel (b): deuteron mass fraction X_d as function of the baryon density as determined by employing the same sets of parameters of panel (a). In both panels, the DD2 nucleon-meson effective interaction, with properly rescaled meson coupling strengths at saturation, is adopted

The sets of parameters DD2-d3, DD2- $\chi d1$, DD2- $\chi d2$, and DD2- $\chi d3$ listed in Table 2 return a smooth behavior of the mass fraction for the whole range of baryon densities and for any asymmetry. Thus, they will be employed in the next section to study various properties, both for SNM and ANM.

5 Thermodynamic quantities

Once the density behavior of the mass shift and of the corresponding deuteron mass fraction is determined, it is interesting to see how the embedding of quasi-clusters at supra-saturation densities affects some general thermodynamic quantities.

5.1 SNM: EoS and incompressibility

Let us focus in this section on the results for SNM. The density dependence of the energy per nucleon E/A is plotted in Fig. 8. The sets of parameters DD2-d3, DD2- $\chi d1$, DD2- $\chi d2$, DD2- $\chi d3$ listed in Table 2 are employed. The standard DD2 parameterization, describing the deuteron free case, is also shown as reference for comparison. The inset of Fig. 8 depicts in particular the differences between the energy per nucleon derived with each set and the chosen reference. First of all, one notices that, in light of the fit performed at saturation, all the curves remain rather close in the low-density regime. However, the parameterizations with deuterons differ from the standard DD2 result in the zero-density limit, approaching one half of the deuteron binding energy in vacuum. Moreover, remarkable differences also emerge in the

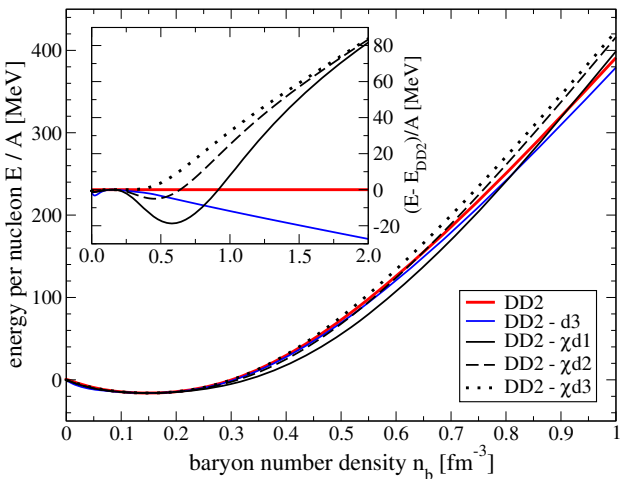


Fig. 8 Energy per nucleon as a function of the baryon density, as determined by employing four selected set of parameters listed in Table 2, for the mass shift parameterization given in Eqs. (58)–(61). For comparison, the curve obtained for the DD2 parameterization in the deuteron-free case is also shown, as the red full line. The inset shows the differences with respect to the predictions of the standard DD2 parameterization in a larger baryon density range

high-density behavior of the energy per nucleon. Despite the fit performed at saturation, as in Fig. 5, a stronger binding is generally observed in the neighbourhood of n_0 in the parameterizations accounting for the presence of deuterons. This stronger attraction persists also to all densities in the case of the DD2-d3 set, despite the disappearance of the deuterons which is expected to occur at n_b around 0.45 fm^{-3} with this parameterization (see Fig. 6). The reduction in the energy per nucleon observed at higher densities with the DD2-d3 is thus only driven by the changed balance between the scalar and vector components, which is a result of the rescaling of the meson coupling strengths at saturation.

A different scenario manifests itself with the parameterizations derived with a reduced scaling factor χ . There, no systematic increased binding, as compared to the DD2 case, is observed. A delicate interplay takes place between the stronger attraction, which is produced by the presence of the deuterons, and the repulsion determined by the increased stiffness of the EoS. This is a result of the modification introduced in the strengths of the σ and ω meson couplings. A global repulsive contribution is seen at large baryon densities, while a significant reduction of the energy per nucleon might be observed up to approximately $3n_0$, depending on the value reached by the deuteron mass fraction in correspondence of the local maximum observed in Fig. 7. However, as highlighted in the inset of Fig. 8, the three black curves converge in the asymptotic limit, where a smooth disappearance of the clusters was depicted in panel (b) of Fig. 6.

The incompressibility characterizes the curvature of the energy per nucleon. It is defined here as

$$K(n_b) = 9n_b^2 \frac{\partial^2(E/A)}{\partial n_b^2} \quad (64)$$

through a second derivative with respect to the baryon density.¹ We recall that the incompressibility was not constrained within the approach adopted in this work. A constraint on the incompressibility would translate to a constraint on the second density derivative of the mass shift at saturation. In addition, it would require, as a further input at saturation, the knowledge of the density derivative of the deuteron mass fraction. Although some numerical analyses have suggested that SRC pairs have a minimum in the neighbourhood of the saturation, owing to the interplay between the tensor component and the repulsive core of the nuclear force [49–51], we preferred to prescind from applying such a constraint. Instead, the predictions for the density behavior of K are numerically extracted from the energy per nucleon. They are plotted in Fig. 9 for the four selected parameterizations of Table 2 considered before. The related inset shows the differences with respect to the standard DD2 reference, which is also shown in the main plot for comparison. As a general feature, one observes that a softening of the EoS is recovered in the region beyond saturation, up to a density around $3n_0$. Furthermore, the size of this effect depends on the magnitude of the deuteron mass fraction.

As clearly evidenced in Table 3, the predictions for the incompressibility at saturation lie within or below the range of values generally assumed for this quantity [82–85] for all the parameterizations here employed. Strong differences are observed in the high-density region, depending on the value for the scaling factor χ . A much stiffer EoS is envisaged in particular at very large baryon densities, when a scaling factor $\chi = 1/\sqrt{2}$ is assumed, as a consequence of the significant change introduced in the balance between the scalar and the vector components in this case.

Fig. 9 also exhibits another aspect to be discussed. The blue curve, which corresponds to the DD2-d3 parameterization, reveals the emergence of a discontinuity at a baryon density around 0.45 fm^{-3} . This striking feature signals the abrupt disappearance of the cluster, which was observed in Fig. 6, panel (b) and already discussed before. It is worthwhile to mention that a discontinuity in the matter incompressibility or in any other quantity related to the second derivative of a thermodynamic potential is the signature for the possible emergence of a second-order phase transition. One notices, by the way, that this feature is in complete analogy to the

¹ The original definition of K uses a second derivative with respect to the Fermi momentum and gives different results as compared to the definition used here but can not be used at finite temperatures. However, both definitions coincide at saturation.

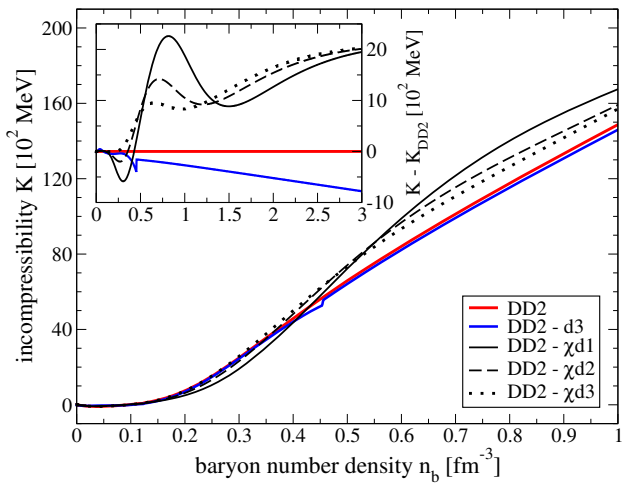


Fig. 9 Incompressibility K as a function of the baryon density as determined by employing four selected set of parameters listed in Table 2 and for the mass shift parameterization given in Eqs. (58)–(61). For comparison, the curve obtained for the DD2 parameterization in the deuteron-free case is also shown as the red full line. The inset shows the differences with respect to the predictions of the standard DD2 parameterization in a larger baryon density range

Table 3 Values of the incompressibility K_0 , in MeV, at saturation density as derived according to Eq. (64), for four selected parameterizations employed in this work. The result for the DD2 is also given for comparison

	DD2	DD2-d3	DD2- χ d1	DD2- χ d2	DD2- χ d3
K_0 [MeV]	242.7	199.6	185.3	207.3	240.3

disappearance of pairing correlations that was observed in previous works at low density [86, 87]. Another discontinuity would emerge moreover at larger densities, if the calculation with the DD2-d3 parameterization is not stopped when the cluster dissolves, so that a further reappearance of the deuterons at higher density is allowed. The inset of Fig. 9 shows that no discontinuity is instead observed when the deuteron mass fraction smoothly decreases with the density. The latter situation may however occur only for the parameterizations characterized by a reduced value of the scaling factor χ .

5.2 Predictions for ANM

5.2.1 Deuteron mass fraction and EoS

Let us finally concentrate on the predictions for ANM. In Fig. 10, panel (a), the density dependence of the deuteron mass fraction is plotted for different values of the isospin asymmetry $|\beta|$. The DD2- χ d1 parameterization is employed for sake of illustration. The adopted parameterization allows one to get the largest value for the deuteron mass fraction around

the local maximum, which was observed beyond 0.5 fm^{-3} in panel (b) of Fig. 7. In such a way, the effect of embedding the quasi-deuterons at supra-saturation densities is better emphasized. However, similar results, at least from a qualitative point of view, would be obtained with the other sets of parameters accounting for the presence of the deuterons. The red line indicates the maximum allowed deuteron mass fraction values, which are compatible with a non negative value of the Dirac effective mass of the nucleons. Let us recall that this curve corresponds to $X_d = \min\{1 - |\beta|, X_d^{(\max)}\}$, so that it evolves with $|\beta|$. Then only the border for SNM ($\beta = 0$) is plotted in panel (a) of Fig. 10 to avoid to overload the figure.

As a quite interesting result, Fig. 10 highlights that, although the mass shift function defined in Eqs. (58)–(61) has no explicit dependence on the isospin asymmetry, the corresponding deuteron mass fraction evolves with $|\beta|$, giving rise to a continuous overall reduction when increasing the neutron-proton asymmetry of the matter. Moreover, the smooth transition to the cluster-free matter realized in SNM with the DD2- χ d1 is preserved also in the ANM case.

The density behavior of the energy per nucleon is depicted in panel (b) of Fig. 10, for the same parameterization and the same asymmetry values considered in panel (a). The inset of panel (b) displays moreover the difference in the energy per nucleon, as determined with the DD2- χ d1 and the DD2 parameterization. Although not clearly visible, differently than in the deuteron-free DD2 case, the zero-density limit does not approach zero, except for the PNM case ($\beta = 1$) in which deuterons are obviously not formed. This feature will be more visible below, when studying the symmetry energy.

The results shown in the inset of panel (b) help to disentangle the effect induced on the stiffness of the EoS, owing to the rescaling of the meson couplings at saturation and the changes ascribable to the presence of the deuterons. The curve related to $|\beta| = 1$, being characterized by $X_d = 0$, demonstrates that, apart from a tiny enhancement of the attraction below saturation (not clearly visible in the figure), a much more repulsive PNM EoS is produced for DD2- χ d1 beyond saturation as compared to DD2. This is the result of the modification induced on the effective interaction by changing the meson coupling strengths. However, for the curves characterized by smaller asymmetry values, such a repulsion is counterbalanced by the attraction produced by the deuterons. An interplay analogous to the one discussed in the SNM case takes place. In such a way, a reduction of the energy per nucleon of ANM might be observed with the DD2- χ d1 parameterization, in the intermediate density region beyond saturation. This region may actually extend up to very large densities, close to $n_b = 0.9 \text{ fm}^{-3}$ in SNM. On the other hand, in the asymptotic limit the quasi-deuterons tend to dissolve, so that their extra-binding vanishes and the black curves depicted in the inset converge to the $|\beta| = 1$ one.

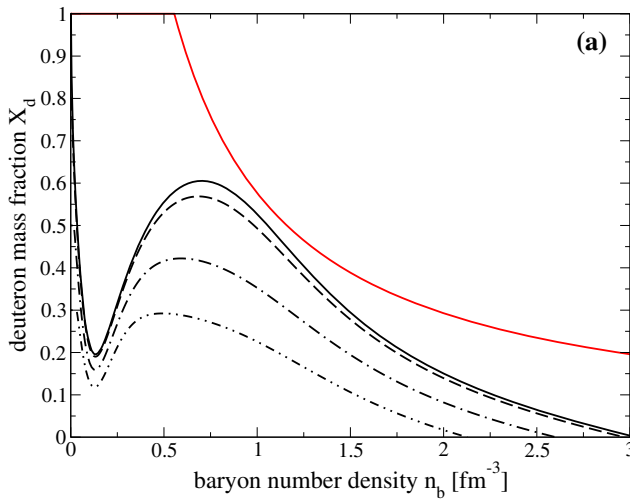
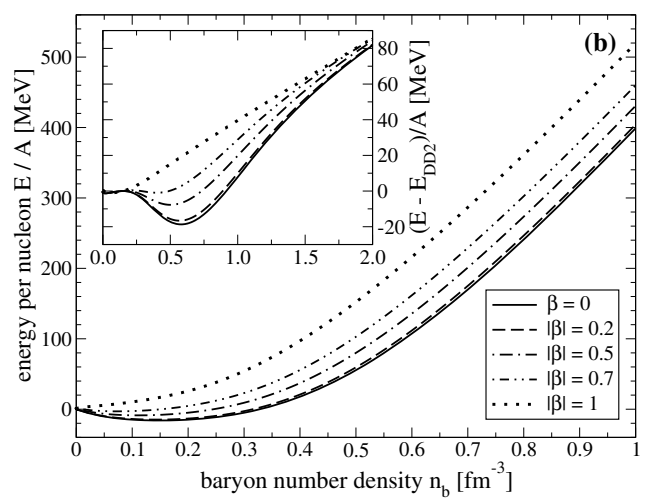


Fig. 10 Panel (a): deuteron mass fraction X_d as function of the baryon density, as determined by employing the DD2- χ d1 parameterization. The results for SNM ($\beta = 0$) are compared with the corresponding ones deduced with different values of the asymmetry $|\beta|$. Panel (b): Energy per nucleon as a function of the baryon density, as determined



by employing the same parameterization and the same asymmetry values as in panel (a). The inset shows the difference of the energy per nucleon between the DD2- χ d1 and DD2 parameterizations for the same asymmetry values, in a wider range of baryon densities

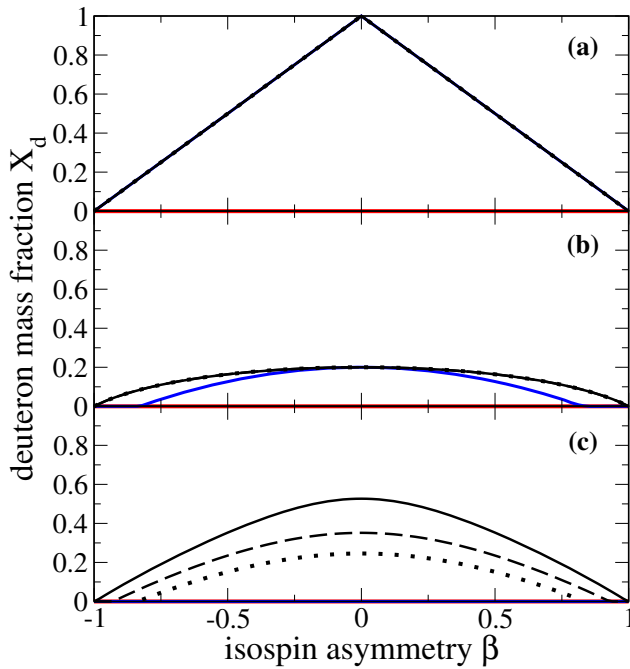
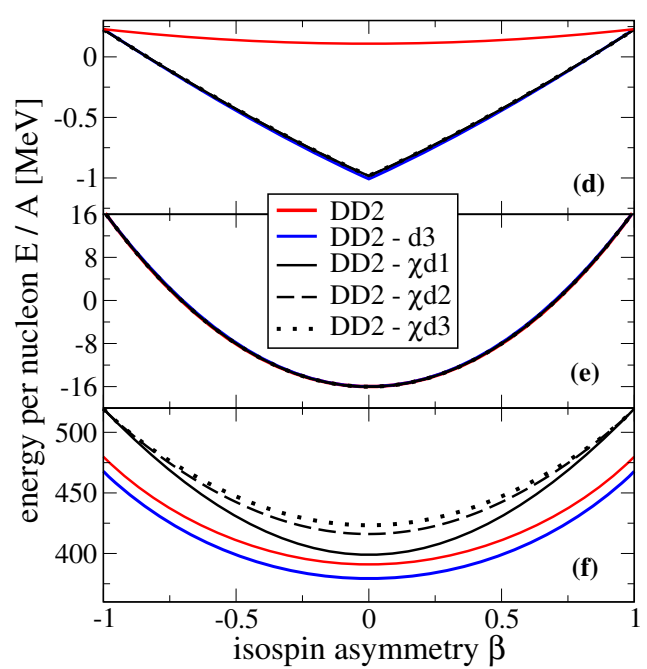


Fig. 11 Left panels: Deuteron mass fraction as function of the isospin asymmetry β , for four selected parameterizations accounting for the presence of the deuterons considered in this work. Right panels: Energy per nucleon as a function of β as determined by employing the same parameterizations as in the left panels. For comparison, the curve



obtained for the DD2 parameterization in the deuteron-free case is also shown. Three different values of the total baryon density are considered: $n_b^{(\text{low})} = 10^{-4} \text{ fm}^{-3}$ (panels (a) and (d)), n_0 (panels (b) and (e)) and $n_b^{(\text{high})} = 10^0 \text{ fm}^{-3}$ (panels (c) and (f))

A further insight into the dependence of the deuteron mass fraction and the energy per nucleon on the isospin asymmetry might be achieved by looking at Fig. 11. Three different values of the total baryon density are considered:

$n_b^{(\text{low})} = 10^{-4} \text{ fm}^{-3}$ (panels (a) and (d)), n_0 (panels (b) and (e)) and $n_b^{(\text{high})} = 10^0 \text{ fm}^{-3}$ (panels (c) and (f)). The standard DD2 parameterization is also plotted in the right panels.

First of all, one observes that all the quantities are symmetric with respect to the SNM ($\beta = 0$) case. At the lowest density value considered in Fig. 11, $n_b^{(\text{low})}$, the deuteron fraction X_d equals the maximum allowed fraction and behaves thus like $X_d = 1 - |\beta|$, for the parameterizations accounting for the presence of the deuterons. As a result, a characteristic triangular shape of X_d and E/A is observed in panels (a) and (d). The energy per nucleon does not follow the standard parabolic law which is predicted in the deuteron-free DD2 case and reaches smaller values in SNM. It approaches half of the deuteron binding energy in vacuum in the zero-density limit. The energy per nucleon determined with the parameterizations accounting for the deuterons coincides with the DD2 result only for matter composed exclusively of neutrons or protons.

Secondly, a different picture is observed at the saturation density n_0 . There, by varying the isospin asymmetry, the deuteron mass fraction departs from the value $X_d = 0.2$ imposed for $\beta = 0$ (see panel (b)). A mild dependence of the deuteron mass fraction on β is assessed for the parameterization characterized by a reduced scaling factor χ . A larger sensitivity exists in the case of the DD2-d3 parameterization. Let us recall that, for this parameterization, the clusters disappear for SNM at density around 0.45 fm^{-3} . Panel (b) shows that the clusters may dissolve already at saturation density for finite β values, at least in the case of the DD2-d3 parameterization. On the other hand, the presence of the deuteron persists at n_0 for all asymmetry values except $|\beta| = 1$, for parameterizations with $\chi = 1/\sqrt{2}$. However, the parabolic dependence of the energy per nucleon on the isospin asymmetry of the DD2 parameterization is perfectly reproduced with all the considered parameterizations. This result is clearly shown in panel (e). It originates from the requirement to keep the energy per nucleon at saturation constrained, both for SNM and for matter composed exclusively of neutrons or protons.

Thirdly, it is interesting to discuss what happens at the highest density value, $n_b^{(\text{high})}$, considered in Fig. 11, panels (c) and (f). Here, different results are obtained among the parameterizations characterized by a scaling factor $\chi = 1/\sqrt{2}$. However, for this density value, the deuterons survive at all asymmetries only with the DD2- χ d1 parameterization, for which the largest value was already predicted in the SNM case. For the other two parameterizations with $\chi = 1/\sqrt{2}$, the clusters dissolve already for $|\beta|$ values smaller than 1. On the other hand, since $n_b^{(\text{high})}$ lies beyond the density at which the cluster dissolution is predicted in SNM, the deuteron mass fraction identically vanishes in case of the DD2-d3 parameterization. The corresponding asymmetry dependence of the energy per nucleon, which is depicted in panel (f), is then driven only by the modification in the coupling strengths which was needed to keep the saturation properties well

constrained. As in Fig. 8, a slightly larger attraction is foreseen with the DD2-d3 parameterization, with respect to the DD2 reference case. The opposite happens instead when the parameterizations with a reduced value of the scaling factor are considered. In this case, a stronger repulsion is envisaged, partially mitigated, at least for small asymmetry values, by the stronger binding provided by the presence of deuterons. Quite interestingly, one observes that the parameterizations plotted by black curves always converge when approaching $|\beta| = 1$, where $X_d = 0$. A change of the parameterization, which implies an according change of the deuteron fraction at supra-saturation densities, affects the curvature of the dependence of the energy per nucleon on β and thus the symmetry energy. The latter quantity will be studied in detail below.

5.2.2 Symmetry energy and its slope

In the present work, the symmetry energy J is calculated as the difference between the energies per nucleon in PNM and SNM

$$J(n_b) = \frac{E}{A} \bigg|_{\beta=1} (n_b) - \frac{E}{A} \bigg|_{\beta=0} (n_b). \quad (65)$$

The quantity obtained through this equation is identical to the symmetry energy calculated from the usual definition

$$J(n_b) = \frac{1}{2} \frac{\partial^2 (E/A)}{\partial \beta^2} \bigg|_{\beta=0} \quad (66)$$

using a second derivative of the energy per nucleon with respect to the asymmetry, if E/A follows a quadratic dependence on β . The density dependence of J is plotted in Fig. 12, panel (a). The inset of panel (a) shows a zoom at sub-saturation densities. Once again, the inset highlights the dissimilar behavior in the zero density limit, when the presence of the clusters is taken into account or not. It reflects the differences existing in the very dilute regime of the SNM EoS with respect to the deuteron-free case. If clustering is taken into account, the symmetry energy approaches indeed half of the deuteron binding energy in the zero-density limit in contrast to the simple description without explicit two-particle correlations. Some differences emerge among the parameterizations which account for the presence of the deuterons below n_0 . Apart from the constraint at saturation, no restrictions have been imposed on the density behavior of J .

Concerning the behavior beyond saturation density, despite the presence of the deuterons, at least up to 0.45 fm^{-3} , the blue curve remains close to the result of the standard DD2 parameterization. Huge differences are instead observed in the supra-saturation density region when the parameterizations with a reduced value of the deuteron-meson coupling scaling factor is considered. Furthermore, the size of the effect depends quite strongly on the mass fraction of the deuterons. The differences vanish in the asymptotic limit,

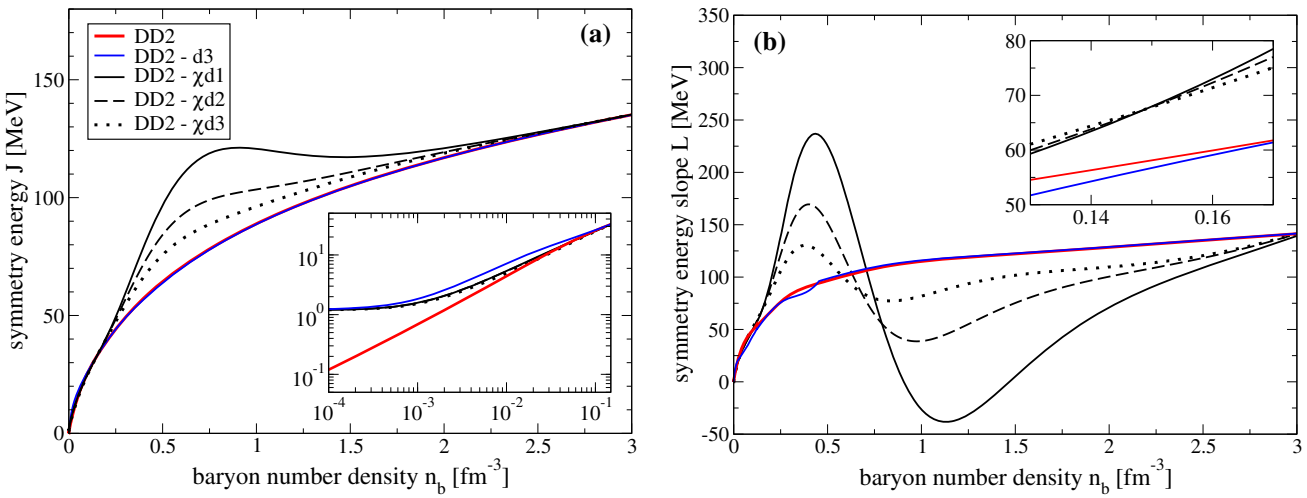


Fig. 12 Panel (a): symmetry energy J as function of the baryon density, as determined through Eq. (65) for four selected parameterizations employed in this work. The inset shows a zoom around the saturation density n_0

density, as determined through Eq. (67), for the same parameterizations as in panel (a). The inset shows a zoom around the saturation density n_0

where the deuterons disappear. The black and blue curves approach the result of the standard DD2 parameterization as the contribution of the ρ meson to the symmetry energy vanishes due to the suppression of its coupling, leaving the imbalance of the Fermi momenta of the nucleons as the main contribution to J .

Finally, it is interesting to look at the density derivative of the curves plotted in panel (a). The slope L of the symmetry energy is numerically calculated here as

$$L(n_b) = 3n_b \frac{dJ}{dn_b} \quad (67)$$

and the result is shown in Fig. 12, panel (b). Except for the different behavior in the zero-density limit, the blue curve roughly coincides with the standard DD2 in the whole range of densities. A small kink is only observed for the DD2-d3 parameterization around 0.45 fm⁻³. This kink is related to the disappearance of the deuterons in the SNM case. We recall that this feature was also responsible for the emergence of the discontinuity in the matter incompressibility discussed before. A huge double oscillation around the result obtained with the standard DD2 parameterization is observed for the parameterizations with a reduced scaling factor χ . The magnitude of this oscillation depends again on the deuteron mass fraction predicted at supra-saturation densities, thus reflecting the result shown in panel (a) of Fig. 12. The inset of panel (b) displays the predictions for the symmetry energy slope around saturation. In spite of the extremely large differences in the high-density regime, reasonable values are obtained at saturation density with all the parameterizations considered in this work. These values, which are collected in Table 4, lie within the range usually assumed for the slope of the

Table 4 Values of the slope of the symmetry energy L_0 , in MeV, at saturation density as derived according to Eq. (67), for four selected parameterizations employed in this work. The result for the DD2 is also given for comparison

	DD2	DD2-d3	DD2- χ d1	DD2- χ d2	DD2- χ d3
L_0 [MeV]	57.94	56.49	67.50	67.50	67.50

symmetry energy, see, e.g., [88] and references therein. The three black curves, crossing each other at saturation, naturally provide the same value. Alternative scenarios manifest for the high-density behavior of the symmetry energy and its slope. The stiffness of the EoS in the supra-saturation density regime turns out to be strongly affected by the value of the scaling factor. It is less dependent on the mere presence of the deuterons. Thus, as a general feature, one concludes that smaller values of the scaling factor correspond to higher stiffness values in the density region beyond saturation relevant for the applications of the model.

6 Conclusions and outlook

In this paper, we have proposed and explored a novel approach to embed SRCs within the GRDF, a well-established phenomenological EDF based on nucleon and cluster degrees of freedom. In such a way, we aim to overcome the inconsistencies between recent experimental evidences, which brought to light the existence of SRCs, and the predictions of phenomenological models derived from mean-field approaches without explicit correlations at densities around

saturation. Previous generalisations of these EDFs represent many-body correlation by cluster which dissolve, by construction, when the nuclear saturation density is approached from below. Within an extended relativistic mean-field model with density dependent couplings, the idea of this work was to effectively account for the existence of SRCs through proper in-medium modifications of the cluster properties around saturation and above. They are considered as quasi-particles with density-dependent binding energies. Quasi-deuterons immersed in dense matter are used as surrogate for correlations in this first exploratory step. For the time being, the zero temperature case, where the deuteron fraction is determined by the density of a boson condensate, was addressed.

Suitable parameterizations of the cluster mass shift were derived, for the first time, for all baryon densities. The proposed mass shift functions comply with the available constraints and were employed to determine the density dependence of the quasi-deuteron mass fraction at arbitrary isospin asymmetries, thus for symmetric as well as for asymmetric nuclear matter. They were constrained by microscopic many-body calculations in the low-density limit, by specifying the actual deuteron fraction at saturation and by assuming a deuteron mass fraction behavior that respects the boson condensation condition at higher densities. The effective deuteron fraction around saturation was specified by extrapolating the experimental results on SRC pairs in nuclei to infinite nuclear matter. Further constraints were moreover imposed at supra-saturation densities by the maximum allowed deuteron fraction, compatible with a non-negative value of the Dirac effective mass of the nucleons.

A proper description of well-constrained nuclear matter quantities at saturation required a refit of the nucleon-meson coupling strengths. An important role of the coupling scaling factor χ was revealed. It rules the coupling strength of the mesons with nucleons bound in the clusters. Such a scaling factor plays actually a primary role in the whole analysis developed in this work.

The natural choice was supposed to be that the nucleons inside the deuterons couple to the mesons with the same strength as the unbound nucleons. However, with this choice, the deuteron mass shift is not a monotonic function of the deuteron mass fraction for all baryon densities. As a result, the relation between the mass shift and the deuteron mass fraction can not be inverted uniquely in all cases. The same holds for any scaling factor χ larger than $1/\sqrt{2}$. Thus, as possible extreme values of two well distinct behaviors, two different values of the scaling factor, namely $\chi = 1$ and $\chi = 1/\sqrt{2}$ were chosen, in the calculations performed in this work. The latter value is however significantly smaller than the universal scaling factor for the cluster-meson coupling strength. A value smaller than $\chi = 1$ was proposed in previous calculations of the EoS to take into account in-medium effects and to get a good description of the chemical

equilibrium constants determined from recent experimental data.

As a general feature, our analysis shows that, for $\chi = 1$, the only possible smooth solution for the density dependence of the deuteron mass fraction implies a sudden disappearance of the clusters at a density below the one corresponding to the emergence of a pole. In correspondence of this density, a discontinuity in the matter incompressibility emerges, analogous to the one observed at low density, owing to the disappearance of the pairing correlations and indicating the emergence of a second order phase transition. The analogy between the behavior of pairing and SRCs deserves however further investigation. For $\chi = 1$, the density where the pole emerges is located around three times the saturation density. However, for more realistic values of the scaling factor, the pole is expected to appear at much higher densities, thus much beyond the range that is relevant in applications of the model. When the scaling factor value $\chi = 1/\sqrt{2}$ is considered, alternative solutions exist, permitting smooth functions of the density dependence of the deuteron mass fraction for all densities. Three different parameterizations, providing such a smooth behavior and characterized by different maximum deuteron fraction values at supra-saturation densities, were proposed.

Striking effects on some thermodynamic quantities are recognized, owing to the presence of the quasi-deuterons in the neighbourhood of saturation and at supra-saturation densities. In particular, a softening of the SNM EoS is systematically observed with respect to the standard DD2 parameterization, which does not include deuteron-like correlations. However, the stronger attraction, which is produced by the presence of the deuterons, might be counterbalanced by the repulsion driven by the modified coupling strengths. This delicate interplay is additionally tuned by the value of the scaling factor, which determines then alternative scenarios for the high-density behavior of the symmetry energy and its slope. In general, one concludes that smaller values of the scaling factor correspond to higher stiffness of the EoS in the supra-saturation density regime.

Last, but not least, it is worthwhile to recall that our analysis permits to also recover the correct low-density limit of the EoS. Indeed, at zero-density, both the energy per nucleon of SNM and the symmetry energy tend to be equal to one half of the deuteron binding energy in vacuum, in contrast to the predictions of standard mean-field models without cluster correlations.

The findings of the present study represent a first step to improve the description of nuclear matter and its EoS at supra-saturation densities in EDFs by considering correlations in an effective way. In a next step, the single-particle momentum distributions can be explored using proper wave functions of the quasi-deuteron in the medium. They have to be derived consistently with the interaction used in the

model and will lead to prediction of the cluster mass shifts and fractions that can be compared to the suggested forms of the present work. The many-body wave function of a cluster contains correlated nucleons with a specific momentum distribution. Then an imprint on the single-nucleon momentum distribution in nuclear matter is expected, such that a high-momentum tail develops even at zero temperature, as observed in the experimental study of SRCs by nucleon knockout with high-energy electrons.

The present approach can be generalized to finite temperatures, where a further change of the single-nucleon momentum distribution arises owing to the thermal change in the distribution functions. Also a momentum dependence of the mass shift and a more involved dependence on the isospin asymmetry might be considered in a future work, together with the effect of including heavier clusters and to investigate their relative importance.

As a perspective, we finally aim at investigating the effect of SRCs on neutron stars in the EDF framework, similarly to what was done in some prior studies, see, e.g., [62], but our approach is to replace heuristic parameterizations of the momentum distributions with more microscopically founded descriptions.

More in general, we aim at achieving a more comprehensive description of correlations and clustering phenomena, which represents still a challenge from a theoretical point of view, despite the importance of these features in the widest scope of astrophysical applications and for general aspects of reactions dynamics in heavy-ion collisions.

Acknowledgements The authors thank Maria Colonna and Gerd Röpke for their comments and suggestions on this work. We acknowledge support by the Deutsche Forschungsgemeinschaft (DFG - German Research Foundation) and the Open Access Publishing Fund of Technical University of Darmstadt. S. B. acknowledges support from the Alexander von Humboldt foundation.

Funding Information Open Access funding enabled and organized by Projekt DEAL.

Data Availability Statement This manuscript has no associated data or the data will not be deposited. [Authors' comment: This is a theoretical study and there are no experimental data. All model parameters are given in the text and in the tables.]

Open Access This article is licensed under a Creative Commons Attribution 4.0 International License, which permits use, sharing, adaptation, distribution and reproduction in any medium or format, as long as you give appropriate credit to the original author(s) and the source, provide a link to the Creative Commons licence, and indicate if changes were made. The images or other third party material in this article are included in the article's Creative Commons licence, unless indicated otherwise in a credit line to the material. If material is not included in the article's Creative Commons licence and your intended use is not permitted by statutory regulation or exceeds the permitted use, you will need to obtain permission directly from the copyright holder. To view a copy of this licence, visit <http://creativecommons.org/licenses/by/4.0/>.

Appendix A: Mass fraction derivative of the deuteron mass shift

The deuteron mass shift (44) is in general a function of the baryon density n_b , the asymmetry β , the deuteron fraction X_d , and the temperature T . In this section, the derivative of $\Delta m_d^{(\text{high})}$ with respect to X_d is derived for constant n_b and β at $T = 0$. In a first step, the derivative of the nucleon effective chemical potential with respect to X_d is expressed as

$$\frac{\partial \mu_q^*}{\partial X_d} \bigg|_{n_b, \beta} = \frac{1}{\mu_q^*} \left(k_q \frac{\partial k_q}{\partial X_d} \bigg|_{n_b, \beta} + m_q^* \frac{\partial m_q^*}{\partial X_d} \bigg|_{n_b, \beta} \right) \quad (\text{A1})$$

using Eq. (35). The derivative of the Fermi momentum of a nucleon $q = n, p$ is found with help of the relation

$$\frac{\partial n_q^{(v)}}{\partial X_d} \bigg|_{n_b, \beta} = -\frac{n_b}{2} = \frac{3n_q^{(v)}}{k_q} \frac{\partial k_q}{\partial X_d} \bigg|_{n_b, \beta} \quad (\text{A2})$$

for the vector density (19). Using Eqs. (A1) and (A2), the derivative of the scalar density of the nucleons can be written as

$$\frac{\partial n_q^{(s)}}{\partial X_d} \bigg|_{n_b, \beta} = -\frac{n_b}{2} \frac{m_q^*}{\mu_q^*} + f_q \frac{\partial m_q^*}{\partial X_d} \bigg|_{n_b, \beta} \quad (\text{A3})$$

with the factor

$$f_q = 3 \left(\frac{n_q^{(s)}}{m_q^*} - \frac{n_q^{(v)}}{\mu_q^*} \right) \quad (\text{A4})$$

after several steps of recasting the individual contributions. Eq. (A3) contains again the derivative of the effective mass that assumes the simple form

$$\frac{\partial m_q^*}{\partial X_d} \bigg|_{n_b, \beta} = -C_\sigma \frac{\partial n_\sigma}{\partial X_d} \bigg|_{n_b, \beta} \quad (\text{A5})$$

because C_σ depends only on n_b . With the derivatives

$$\frac{\partial n_d^{(v)}}{\partial X_d} \bigg|_{n_b, \beta} = \frac{\partial n_d^{(s)}}{\partial X_d} \bigg|_{n_b, \beta} = \frac{n_b}{2} \quad (\text{A6})$$

of the deuteron densities, the derivative of the σ meson source density (11) is found as

$$\frac{\partial n_\sigma}{\partial X_d} \bigg|_{n_b, \beta} = \frac{n_b}{1 + (f_n + f_p) C_\sigma} \mathcal{U}_d \quad (\text{A7})$$

with

$$\mathcal{U}_d = \chi_{d\sigma} - \frac{m_{\text{nuc}}^*}{2} \left(\frac{1}{\mu_n^*} + \frac{1}{\mu_p^*} \right) \quad (\text{A8})$$

whereas

$$\frac{\partial n_\omega}{\partial X_d} \bigg|_{n_b, \beta} = -n_b (1 - \chi_{d\omega}) \quad (\text{A9})$$

for the source density of the ω meson. Finally, the derivative of the mass shift with respect to the mass fraction is obtained in the compact form

$$\frac{\partial \Delta m_d^{(\text{high})}}{\partial X_d} \Big|_{n_b, \beta} = \left[\frac{2C_\sigma}{1 + (f_n + f_p)C_\sigma} \mathcal{U}_d^2 - \frac{\pi^2}{2\mu_n^* k_n} - \frac{\pi^2}{2\mu_p^* k_p} \right] n_b \quad (\text{A10})$$

with a contribution from the σ meson and kinetic terms.

Appendix B: Density derivative of deuteron mass shift

In this section, the derivative of $\Delta m_d^{(\text{high})}$ with respect to n_b is derived for an arbitrary function $X_d(n_b)$ and constant β at $T = 0$. It requires again several steps. First, the derivatives of the source densities have to be determined. For the ω meson one finds

$$\frac{\partial n_\omega}{\partial n_b} \Big|_\beta = 1 - (1 - \chi_{d\omega}) Y_d \quad (\text{B1})$$

with the quantity

$$Y_d = \frac{\partial (n_b X_d)}{\partial n_b} \Big|_\beta = X_d + n_b \frac{\partial X_d}{\partial n_b} \Big|_\beta \quad (\text{B2})$$

that contains the derivative of the deuteron mass fraction. For the σ meson, the calculation is more involved. Here, the relations

$$\begin{aligned} \frac{\partial n_\sigma}{\partial n_b} \Big|_\beta &= (f_n + f_p) \frac{\partial m_{\text{nuc}}^*}{\partial n_b} \Big|_\beta + \chi_{d\sigma} Y_d \\ &+ \frac{m_{\text{nuc}}^*}{2\mu_n^*} (1 + \beta - Y_d) + \frac{m_{\text{nuc}}^*}{2\mu_p^*} (1 - \beta - Y_d) \end{aligned} \quad (\text{B3})$$

with the factor f_q defined in Eq. (A4) and

$$\frac{\partial m_{\text{nuc}}^*}{\partial n_b} \Big|_\beta = -C_\sigma \frac{\partial n_\sigma}{\partial n_b} \Big|_\beta - C'_\sigma n_\sigma \quad (\text{B4})$$

for the derivative of the effective nucleon mass can be combined to obtain the form

$$\begin{aligned} \frac{\partial n_\sigma}{\partial n_b} \Big|_\beta &= [1 + (f_n + f_p) C_\sigma]^{-1} \\ &\left[- \left(f_n + f_p \right) C'_\sigma n_\sigma + \chi_{d\sigma} Y_d \right. \\ &\left. + \frac{m_{\text{nuc}}^*}{2\mu_n^*} (1 + \beta - Y_d) + \frac{m_{\text{nuc}}^*}{2\mu_p^*} (1 - \beta - Y_d) \right] \end{aligned} \quad (\text{B5})$$

with an explicit dependence on Y_d . In the next step, the derivative of the mass shift assumes the form

$$\begin{aligned} &\frac{\partial \Delta m_d^{(\text{high})}}{\partial n_b} \Big|_\beta \\ &= \frac{k_n}{\mu_n^*} \frac{\partial k_n}{\partial n_b} \Big|_\beta + \frac{k_p}{\mu_p^*} \frac{\partial k_p}{\partial n_b} \Big|_\beta + \left(\frac{1}{\mu_n^*} + \frac{1}{\mu_p^*} \right) m_{\text{nuc}}^* \frac{\partial m_{\text{nuc}}^*}{\partial n_b} \Big|_\beta \\ &+ 2(1 - \chi_{d\omega}) \left(C_\omega \frac{\partial n_\omega}{\partial n_b} \Big|_\beta + C'_\omega n_\omega \right) \\ &+ 2\chi_{d\sigma} \left(C_\sigma \frac{\partial n_\sigma}{\partial n_b} \Big|_\beta + C'_\sigma n_\sigma \right) \end{aligned} \quad (\text{B6})$$

with

$$\frac{\partial k_n}{\partial n_b} \Big|_\beta = \frac{k_n}{3n_n^{(v)}} \left(\frac{1 + \beta - Y_d}{2} \right) \quad (\text{B7})$$

and

$$\frac{\partial k_p}{\partial n_b} \Big|_\beta = \frac{k_p}{3n_p^{(v)}} \left(\frac{1 - \beta - Y_d}{2} \right). \quad (\text{B8})$$

Using the expressions (B1) and (B5), the final result can be expressed in compact form as

$$\frac{\partial \Delta m_d^{(\text{high})}}{\partial n_b} \Big|_\beta = \mathcal{W}_d - \mathcal{Z}_d Y_d \quad (\text{B9})$$

with the auxiliary quantities

$$\begin{aligned} \mathcal{Z}_d &= \frac{\pi^2}{2\mu_n^* k_n} + \frac{\pi^2}{2\mu_p^* k_p} + 2(1 - \chi_{d\omega})^2 C_\omega \\ &- \frac{2C_\sigma}{1 + (f_n + f_p) C_\sigma} \mathcal{U}_d^2 \end{aligned} \quad (\text{B10})$$

$$\begin{aligned} \mathcal{W}_d &= \frac{\pi^2}{2\mu_n^* k_n} (1 + \beta) + \frac{\pi^2}{2\mu_p^* k_p} (1 - \beta) \\ &+ 2(1 - \chi_{d\omega}) (C_\omega + C'_\omega n_\omega) \\ &+ \frac{2}{1 + (f_n + f_p) C_\sigma} \mathcal{U}_d \\ &\left[C'_\sigma n_\sigma + C_\sigma \frac{m_{\text{nuc}}^*}{2} \left(\frac{1 + \beta}{\mu_n^*} + \frac{1 - \beta}{\mu_p^*} \right) \right] \end{aligned} \quad (\text{B11})$$

and \mathcal{U}_d as given in (A8).

Appendix C: Conversion of parameters at saturation

In order to find the coupling strengths $\Gamma_{\sigma,0}$ and $\Gamma_{\omega,0}$ as well as the deuteron mass shift and its density derivative at saturation, a step-by-step procedure can be followed. These quantities are determined as soon as the saturation density n_0 , the binding energy per nucleon B_0 , the effective nucleon mass $m_{\text{nuc},0}^*$ and deuteron fraction $X_{d,0}$ of SNM are specified.

In a first step, the scalar and vector densities

$$n_{d,0}^{(s)} = n_{d,0}^{(v)} = n_0 \frac{X_{d,0}}{2} \quad (C1)$$

of the deuteron and the total vector density

$$n_{\text{nuc},0}^{(v)} = n_0 (1 - X_{d,0}) \quad (C2)$$

of the nucleons are immediately obtained from n_0 and $X_{d,0}$ in SNM. Then the Fermi momentum

$$k_{\text{nuc},0} = \left[\frac{6\pi^2}{g_{\text{nuc}}} n_{\text{nuc},0}^{(v)} \right]^{1/3} \quad (C3)$$

with degeneracy factor $g_{\text{nuc}} = 4$ and the effective chemical potential

$$\mu_{\text{nuc},0}^* = \sqrt{k_{\text{nuc},0}^2 + (m_{\text{nuc},0}^*)^2} \quad (C4)$$

allow to calculate the scalar density

$$\begin{aligned} n_{\text{nuc},0}^{(s)} & \frac{g_{\text{nuc}} m_{\text{nuc},0}^*}{4\pi^2} \\ & = \left[k_{\text{nuc},0} \mu_{\text{nuc},0}^* - (m_{\text{nuc},0}^*)^2 \ln \frac{k_{\text{nuc},0} + \mu_{\text{nuc},0}^*}{m_{\text{nuc},0}^*} \right] \end{aligned} \quad (C5)$$

using the effective nucleon mass $m_{\text{nuc},0}^*$. Then the source densities

$$n_{\sigma,0} = n_{\text{nuc}}^{(s)} + 2\chi n_{d,0}^{(s)} \quad (C6)$$

and

$$n_{\omega,0} = n_{\text{nuc}}^{(v)} + 2\chi n_{d,0}^{(v)} \quad (C7)$$

with the deuteron-meson coupling scaling factor χ are found and the pressure contribution

$$p_{\text{nuc},0} = \frac{1}{4} \left[\mu_{\text{nuc},0}^* n_{\text{nuc},0}^{(v)} - m_{\text{nuc},0}^* n_{\text{nuc},0}^{(s)} \right] \quad (C8)$$

of the nucleons can be calculated immediately.

In the next step, the effective nucleon mass determines the scalar potential

$$S_{\text{nuc},0} = m_{\text{nuc}} - m_{\text{nuc},0}^* \quad (C9)$$

of the nucleons and thus the scalar coupling

$$C_{\sigma,0} = \frac{S_{\text{nuc},0}}{n_{\sigma,0}} \quad (C10)$$

and finally the coupling strength

$$\Gamma_{\sigma,0} = m_{\sigma} \sqrt{C_{\sigma,0}} \quad (C11)$$

of the σ meson. The binding energy per nucleon B_0 gives the chemical potential

$$\mu_{\text{nuc},0} = m_{\text{nuc}} - B_0 \quad (C12)$$

at saturation and then the vector potential

$$V_{\text{nuc},0} = \mu_{\text{nuc},0} - \mu_{\text{nuc},0}^* \quad (C13)$$

of the nucleons. The latter quantity can be expressed in general as

$$V_{\text{nuc},0} = C_{\omega,0} n_{\omega,0} + C_{\rho,0} n_{\rho,0} + U_0^{(r)} \quad (C14)$$

with the auxiliary quantity

$$U_0^{(r)} = V_0^{(r)} + W_0^{(r)} \quad (C15)$$

that also appears in the total pressure

$$\begin{aligned} P_0 & = p_{\text{nuc},0} + \frac{1}{2} \left(C_{\omega,0} n_{\omega,0}^2 + C_{\rho,0} n_{\rho,0}^2 \right. \\ & \quad \left. - C_{\sigma,0} n_{\sigma,0}^2 \right) + U_0^{(r)} n_0 . \end{aligned} \quad (C16)$$

For SNM, however, the ρ -meson contribution does not appear, since n_{ρ} is identically zero. The two equations (C14) and (C16) allow to solve for the ω coupling

$$\begin{aligned} C_{\omega,0} & = \left(2n_{\omega,0} n_0 - n_{\omega,0}^2 \right)^{-1} \\ & \quad \left(2p_{\text{nuc},0} + 2V_{\text{nuc},0} n_0 - C_{\sigma,0} n_{\sigma,0}^2 \right) \end{aligned} \quad (C17)$$

and further the coupling strength

$$\Gamma_{\omega,0} = m_{\omega} \sqrt{C_{\omega,0}} \quad (C18)$$

using $P_0 = 0$. With known $C_{\sigma,0}$ and $C_{\omega,0}$, their derivatives $C'_{\sigma,0}$ and $C'_{\omega,0}$ can be determined using the same functional density dependence of the couplings as in the reference parameterization. Thus also the rearrangement contribution

$$V_0^{(r)} = \frac{1}{2} \left(C'_{\omega,0} n_{\omega,0}^2 + C'_{\rho,0} n_{\rho,0}^2 - C'_{\sigma,0} n_{\sigma,0}^2 \right) \quad (C19)$$

is given.

Finally, from Eqs. (C14) and (C15) one finds

$$W_0^{(r)} = V_{\text{nuc},0} - C_{\omega,0} n_{\omega,0} - V_0^{(r)} \quad (C20)$$

and the deuteron mass shift derivative

$$\left. \frac{d \Delta m_d}{d n_b} \right|_{n_0} = \frac{W_0^{(r)}}{n_{d,0}^{(s)}} \quad (C21)$$

at saturation. The deuteron mass shift itself is determined as

$$\begin{aligned} \Delta m_{d,0} & = B_d + 2(\mu_{\text{nuc},0}^* - m_{\text{nuc},0}^*) \\ & \quad + 2(1 - \chi_{d\omega}) C_{\omega} n_{\omega} - 2(1 - \chi_{d\sigma}) C_{\sigma} n_{\sigma} \end{aligned} \quad (C22)$$

from the condensation condition with the binding energy of the deuteron in vacuum B_d .

The rescaling of the σ and ω coupling strengths induces a modification of the energy per nucleon in PNM at saturation and thus of the symmetry energy. Within the parabolic

approximation, the symmetry energy at saturation is indeed given by

$$J_0 = \frac{E}{A} \Big|_{n_0, \beta=1} - \frac{E}{A} \Big|_{n_0, \beta=0} = \frac{E}{A} \Big|_{n_0, \beta=1} + B_0. \quad (\text{C23})$$

Then, constraining the value of J_0 implies a constraint on E/A of PNM at n_0 . Taking into account Eq. (31), the condition above writes

$$\mu_{n,0}^* + V_{n,0} - \frac{P_n}{n_0} \Big|_{n_0, \beta=1} = m_{\text{nuc}} + J_0 - B_0 \quad (\text{C24})$$

with the effective chemical potential

$$\mu_{n,0}^* = \sqrt{k_{n,0}^2 + (m_{n,0}^*)^2} \quad (\text{C25})$$

of the neutron at the saturation density n_0 . The effective mass of the neutron $m_{n,0}^* = m_{\text{nuc}} - \Gamma_\sigma n_{n,0}^{(s)}$ has to be determined self-consistently with the scalar density $n_{n,0}^{(s)}$, defined in Eq. (34), using the Fermi momentum $k_{n,0} = (3\pi^2 n_0)^{1/3}$ of the neutron. Since there are no deuterons in PNM, the vector potential of the neutron is given by

$$V_{n,0} = C_{\omega,0} n_\omega + C_{\rho,0} n_\rho + \frac{1}{2} (C'_{\omega,0} n_\omega^2 + C'_{\rho,0} n_\rho^2 - C'_{\sigma,0} n_\sigma^2) \quad (\text{C26})$$

and the pressure assumes the simple form

$$P_n(n_0) = \frac{1}{4} (\mu_{n,0}^* n_{n,0}^{(v)} - m_{n,0}^* n_{n,0}^{(s)}) + \frac{1}{2} [D_{\omega,0} n_\omega^2 + D_{\rho,0} n_\rho^2 - D_{\sigma,0} n_\sigma^2] \quad (\text{C27})$$

with $n_\omega = n_\rho = n_{n,0}^{(v)} = n_0$ and $n_\sigma = n_{n,0}^{(s)}$. The rescaled couplings $C_{\omega,0}$, $C_{\sigma,0}$, $C'_{\omega,0}$, $C'_{\sigma,0}$, $D_{\omega,0}$, and $D_{\sigma,0}$, c.f., Eq. (39), at saturation are already known and thus $C_{\rho,0}$ can be deduced from

$$C_{\rho,0} = \frac{2}{n_0} \left[m_{\text{nuc}} + J_0 - B_0 - \frac{3}{4} \mu_{n,0}^* \right. \\ \left. - \frac{1}{4} m_{n,0}^* \frac{n_{n,0}^{(s)}}{n_0} - \frac{1}{2} C_{\omega,0} n_\omega - \frac{1}{2 n_0} C_{\sigma,0} n_\sigma^2 \right] \quad (\text{C28})$$

and, finally,

$$\Gamma_{\rho,0} = m_\rho \sqrt{C_{\rho,0}} \quad (\text{C29})$$

for the coupling of the ρ meson at saturation.

Appendix D: Analytical expressions for the mass shift parameters

The following analytical expressions permit to calculate the parameters c and d appearing in Eq. (58):

$$c = [1 - \tanh(e)]^{-1}$$

$$\left[\Delta m_{d,0} - \frac{a}{1+b} - f \tanh(g) \right] \quad (\text{D1})$$

$$\eta = [1 - \tanh(e)]^{-1} \left\{ \frac{\partial \Delta m_d}{\partial n_b} \Big|_{n_0} n_0 - \frac{a}{(1+b)^2} + \frac{c e}{\cosh^2(e)} \right. \\ \left. - f \gamma \tanh(g) - \frac{f g}{\cosh^2(g)} - c [1 - \tanh(e)] \right\} \quad (\text{D2})$$

where the values for a , b , e , f and g are determined as explained in Sect. 4.4, while $\Delta m_{d,0}$ and $\frac{\partial \Delta m_d}{\partial n_b} \Big|_{n_0}$ indicate the mass shift and its density slope at saturation density n_0 .

References

1. G. Shen, C. Horowitz, S. Teige, Phys. Rev. C **83**, 035802 (2011). <https://doi.org/10.1103/PhysRevC.83.035802>
2. M. Hempel, T. Fischer, J. Schaffner-Bielich, M. Liebendörfer, Astrophys. J. **748**, 70 (2012). <https://doi.org/10.1088/0004-637X/748/1/70>
3. J.M. Lattimer, M. Prakash, Phys. Rep. **621**, 127 (2016). <https://www.sciencedirect.com/science/article/abs/pii/S0370157315005396?via>
4. B.P. Abbott et al., Phys. Rev. Lett. **121**, 161101 (2018). <https://doi.org/10.1103/PhysRevLett.121.161101>
5. T. Klähn et al., Phys. Rev. C **74**, 035802 (2006). <https://doi.org/10.1103/PhysRevC.74.035802>
6. H. Zheng, S. Burrello, M. Colonna, V. Baran, Phys. Lett. B **769**, 424 (2017). <https://doi.org/10.1016/j.physletb.2017.04.002>
7. H. Zheng, S. Burrello, M. Colonna, D. Lacroix, G. Scamps, Phys. Rev. C **98**, 024622 (2018). <https://doi.org/10.1103/PhysRevC.98.024622>
8. M. Oertel, M. Hempel, T. Klähn, S. Typel, Rev. Mod. Phys. **89**, 015007 (2017). <https://doi.org/10.1103/RevModPhys.89.015007>
9. A. Akmal, V.R. Pandharipande, D.G. Ravenhall, Phys. Rev. C **58**, 1804 (1998). <https://doi.org/10.1103/PhysRevC.58.1804> [arXiv:nucl-th/9804027](https://arxiv.org/abs/nucl-th/9804027)
10. J. Carlson, S. Gandolfi, F. Pederiva, S.C. Pieper, R. Schiavilla, K.E. Schmidt, R.B. Wiringa, Rev. Mod. Phys. **87**, 1067 (2015). <https://doi.org/10.1103/RevModPhys.87.1067> [arXiv:1412.3081](https://arxiv.org/abs/1412.3081) [nucl-th]
11. E. Epelbaum, H.-W. Hammer, U.-G. Meißner, Rev. Mod. Phys. **81**, 1773 (2009). <https://doi.org/10.1103/RevModPhys.81.1773>
12. H.-W. Hammer, S. König, U. Van Kolck, Rev. Mod. Phys. **92**, 025004 (2020). <https://doi.org/10.1103/RevModPhys.92.025004>
13. R.J. Furnstahl, H.W. Hammer, A. Schwenk, Few Body Syst. **62**, 72 (2021). <https://doi.org/10.1007/s00601-021-01658-5> [arXiv:2107.00413](https://arxiv.org/abs/2107.00413) [nucl-th]
14. S. Typel, Phys. Rev. C **89**, 064321 (2014). <https://doi.org/10.1103/PhysRevC.89.064321>
15. J. Tanaka et al., Science **371**, 260 (2021). <https://doi.org/10.1126/science.abe4688>
16. A.R. Raduta, F. Gulminelli, Phys. Rev. C **82**, 065801 (2010). <https://doi.org/10.1103/PhysRevC.82.065801>
17. M. Bender, P.-H. Heenen, P.-G. Reinhard, Rev. Mod. Phys. **75**, 121 (2003). <https://doi.org/10.1103/RevModPhys.75.121>
18. M. Dutra, O. Loureno, J.S. Martins, A. Delfino, J.R. Stone, P. Stevenson, Phys. Rev. C **85**, 035201 (2012). <https://doi.org/10.1103/PhysRevC.85.035201>
19. R. Sellahewa, A. Rios, Phys. Rev. C **90**, 054327 (2014). <https://doi.org/10.1103/PhysRevC.90.054327>

20. M. Dutra et al., Phys. Rev. C **90**, 055203 (2014). <https://doi.org/10.1103/PhysRevC.90.055203>
21. R.J. Furnstahl, Eur. Phys. J. A **56**, 85 (2020). <https://doi.org/10.1140/epja/s10050-020-00095-y>
22. M. Grasso, Prog. Part. Nucl. Phys. **106**, 256 (2019). <https://doi.org/10.1016/j.ppnp.2019.02.002>
23. F. Marino, C. Barbieri, A. Carbone, G. Colò, A. Lovato, F. Pedreira, X. Roca-Maza, E. Vigezzi, Phys. Rev. C **104**, 024315 (2021). <https://doi.org/10.1103/PhysRevC.104.024315>
24. C.J. Yang, M. Grasso, D. Lacroix, Phys. Rev. C **94**, 031301 (2016). <https://doi.org/10.1103/PhysRevC.94.031301>
25. M. Grasso, D. Lacroix, C.J. Yang, Phys. Rev. C **95**, 054327 (2017). <https://doi.org/10.1103/PhysRevC.95.054327>
26. S. Burrello, J. Bonnard, M. Grasso, Phys. Rev. C **103**, 064317 (2021). <https://doi.org/10.1103/PhysRevC.103.064317>
27. S. Burrello, M. Grasso, Eur. Phys. J. A **58**, 1 (2022). <https://doi.org/10.1140/epja/s10050-022-00665-2>
28. C.-J. Yang, M. Grasso, D. Lacroix, Phys. Rev. C **96**, 034318 (2017). <https://doi.org/10.1103/PhysRevC.96.034318>
29. S. Burrello, M. Grasso, C.-J. Yang, Phys. Lett. B **811**, 135938 (2020). <https://doi.org/10.1016/j.physletb.2020.135938>
30. S. Typel, G. Röpke, T. Klähn, D. Blaschke, H.H. Wolter, Phys. Rev. C **81**, 015803 (2010). <https://doi.org/10.1103/PhysRevC.81.015803>
31. S. Burrello, F. Gulminelli, F. Aymard, M. Colonna, A.R. Raduta, Phys. Rev. C **92**, 055804 (2015). <https://doi.org/10.1103/PhysRevC.92.055804>
32. M. Hempel, J. Schaffner-Bielich, Nucl. Phys. A **837**, 210 (2010). <https://www.sciencedirect.com/science/article/abs/pii/S0375947410003325?via>
33. M. Hempel, J. Schaffner-Bielich, S. Typel, G. Röpke, Phys. Rev. C **84**, 055804 (2011). <https://doi.org/10.1103/PhysRevC.84.055804>
34. V. Sagun, A. Ivanytskyi, K. Bugaev, I. Mishustin, Nucl. Phys. A **924**, 24 (2014). <https://www.sciencedirect.com/science/article/abs/pii/S0375947413008117>
35. G. Röpke, L. Münchow, H. Schulz, Phys. Lett. B **110**, 21 (1982). [https://doi.org/10.1016/0370-2693\(82\)90943-1](https://doi.org/10.1016/0370-2693(82)90943-1)
36. G. Röpke, L. Münchow, H. Schulz, Nucl. Phys. A **379**, 536 (1982). [https://doi.org/10.1016/0375-9474\(82\)90013-6](https://doi.org/10.1016/0375-9474(82)90013-6)
37. S. Typel, Eur. Phys. J. Spec. Top. **229**, 3433 (2020). <https://doi.org/10.1140/epjst/e2020-000060-6>
38. H. Pais, S. Typel, in *Nuclear Particle Correlations and Cluster Physics*, ed. by W.-U. Schroeder (World Scientific, Singapore, 2017), pp. 95–133. https://doi.org/10.1142/9789813209350_004
39. N. Fomin et al., Phys. Rev. Lett. **108**, 092502 (2012). <https://doi.org/10.1103/PhysRevLett.108.092502>
40. O. Hen, G.A. Miller, E. Piasetzky, L.B. Weinstein, Rev. Mod. Phys. **89**, 045002 (2017). <https://doi.org/10.1103/RevModPhys.89.045002>
41. J. Arrington, D. Higinbotham, G. Rosner, M. Sargsian, Prog. Part. Nucl. Phys. **67**, 898 (2012). <https://doi.org/10.1016/j.ppnp.2012.04.002>
42. C.C. degli Atti, Phys. Rep. **590**, 1 (2015). <https://doi.org/10.1016/j.physrep.2015.06.002>
43. K.S. Egiyan et al., Phys. Rev. Lett. **96**, 082501 (2006). <https://doi.org/10.1103/PhysRevLett.96.082501>
44. R. Subedi et al., Science **320**, 1476 (2008). <https://doi.org/10.1126/science.1156675>
45. O. Hen et al., Science **346**, 614 (2014). <https://doi.org/10.1126/science.1256785>
46. M. Duer, et al. (collaboration CLAS Collaboration), Nature **560**, 617 (2018). <https://www.nature.com/articles/s41586-018-0400-z>
47. M. Duer, et al., collaboration CLAS Collaboration. Phys. Rev. Lett. **122**, 172502 (2019). <https://doi.org/10.1103/PhysRevLett.122.172502>
48. B. Schmookler et al., Nature **566**, 354 (2019). <https://doi.org/10.1038/s41586-019-0925-9>
49. A. Rios, A. Polls, W. Dickhoff, Phys. Rev. C **89**, 044303 (2014). <https://doi.org/10.1103/PhysRevC.89.044303>
50. Z. Yang, X. Shang, G. Yong, W. Zuo, Y. Gao, Phys. Rev. C **100**, 054325 (2019). <https://doi.org/10.1103/PhysRevC.100.054325>
51. Z.-H. Li, H.-J. Schulze, Phys. Rev. C **94**, 024322 (2016). <https://doi.org/10.1103/PhysRevC.94.024322>
52. B.-J. Cai, B.-A. Li, Phys. Rev. C **93**, 014619 (2016). <https://doi.org/10.1103/PhysRevC.93.014619>
53. B.-A. Li, B.-J. Cai, L.-W. Chen, J. Xu, Prog. Part. Nucl. Phys. **99**, 29 (2018). <https://doi.org/10.1016/j.ppnp.2018.01.001>
54. B.-A. Li, L.-W. Chen, C.M. Ko, Phys. Rep. **464**, 113 (2008). <https://doi.org/10.1016/j.physrep.2008.04.005>
55. P. Russotto et al., Phys. Rev. C **94**, 034608 (2016). <https://doi.org/10.1103/PhysRevC.94.034608>
56. H. Zheng, S. Burrello, M. Colonna, V. Baran, Phys. Rev. C **94**, 014313 (2016). <https://doi.org/10.1103/PhysRevC.94.014313>
57. S. Burrello, M. Colonna, G. Colò, D. Lacroix, X. Roca-Maza, G. Scamps, H. Zheng, Phys. Rev. C **99**, 054314 (2019). <https://doi.org/10.1103/PhysRevC.99.054314>
58. S. Burrello, M. Colonna, H. Zheng, Front. Phys. **7**, 53 (2019). <https://doi.org/10.3389/fphy.2019.00053>
59. L.B. Weinstein, E. Piasetzky, D.W. Higinbotham, J. Gomez, O. Hen, R. Shneor, Phys. Rev. Lett. **106**, 052301 (2011). <https://doi.org/10.1103/PhysRevLett.106.052301>
60. T. Van Cuyck, N. Jachowicz, R. González-Jiménez, M. Martini, V. Pandey, J. Ryckebusch, N. Van Dessel, Phys. Rev. C **94**, 024611 (2016). <https://doi.org/10.1103/PhysRevC.94.024611>
61. W.-M. Guo, B.-A. Li, G.-C. Yong, Phys. Rev. C **104**, 034603 (2021). <https://doi.org/10.1103/PhysRevC.104.034603>
62. H. Lu, Z. Ren, D. Bai, Nucl. Phys. A **1011**, 122200 (2021). <https://doi.org/10.1016/j.nuclphysa.2021.122200>
63. S. Typel, H. Wolter, Nucl. Phys. A **656**, 331 (1999). [https://doi.org/10.1016/S0375-9474\(99\)00310-3](https://doi.org/10.1016/S0375-9474(99)00310-3)
64. O. Buss, T. Gaitanos, K. Gallmeister, H. van Hees, M. Kaskulov, O. Lalakulich, A. Larionov, T. Leitner, J. Weil, U. Mosel, Phys. Rep. **512**, 1 (2012). <https://doi.org/10.1016/j.physrep.2011.12.001>
65. M. Shahrbaf, D. Blaschke, S. Typel, G.R. Farrar, D.E. Alvarez-Castillo (2022). [arXiv:2202.00652](https://arxiv.org/abs/2202.00652) [nucl-th]
66. H. Pais, S. Typel, Comparison of equation of state models with different cluster dissolution mechanisms. In *Nucl. Part. Correl. Clust. Phys.* (World Scientific, 2017) Chapter 4, pp. 95–132. https://doi.org/10.1142/9789813209350_0004
67. S. Typel, D. Alvear Terrero, Eur. Phys. J. A **56**, 160 (2020). <https://doi.org/10.1140/epja/s10050-020-00172-2>
68. M. Ferreira, C. Providencia, Phys. Rev. C **85**, 055811 (2012). <https://doi.org/10.1103/PhysRevC.85.055811> arXiv:1206.0139 [nucl-th]
69. H. Pais, F. Gulminelli, C. Providência, G. Röpke, Phys. Rev. C **97**, 045805 (2018). <https://doi.org/10.1103/PhysRevC.97.045805>
70. H. Pais, F. Gulminelli, C. Providência, G. Röpke, Phys. Rev. C **99**, 055806 (2019). <https://doi.org/10.1103/PhysRevC.99.055806>
71. L. Qin et al., Phys. Rev. Lett. **108**, 172701 (2012). <https://doi.org/10.1103/PhysRevLett.108.172701>
72. H. Pais et al., Phys. Rev. Lett. **125**, 012701 (2020). <https://doi.org/10.1103/PhysRevLett.125.012701>
73. H. Pais et al., J. Phys. G Nucl. Part. Phys. **47**(2020). <https://doi.org/10.1088/1361-6471/aba561>
74. R. Bougault et al., J. Phys. G Nucl. Part. Phys. **47**(2020). <https://doi.org/10.1088/1361-6471/ab56ba>
75. T. Custódio, A. Falcao, H. Pais, C. Providência, F. Gulminelli, G. Röpke, Eur. Phys. J. A **56**, 1 (2020). <https://doi.org/10.1140/epja/s10050-020-00302-w>
76. G. Röpke, Phys. Rev. C **79**, 014002 (2009). <https://doi.org/10.1103/PhysRevC.79.014002>

77. G. Röpke, Nucl. Phys. A **867**, 66 (2011). <https://www.sciencedirect.com/science/article/abs/pii/S037594741100563X?via>
78. G. Röpke, Phys. Rev. C **92**, 054001 (2015). <https://doi.org/10.1103/PhysRevC.92.054001>
79. S. Typel, J. Phys. G **45**, 114001 (2018). <https://doi.org/10.1088/1361-6471/aadea5>
80. M. Wang, G. Audi, A. Wapstra, F. Kondev, M. MacCormick, X. Xu, B. Pfeiffer, Chin. Phys. C **36**, 1603 (2012). <https://doi.org/10.1088/1674-1137/36/12/003>
81. S. Typel, H.H. Wolter, G. Röpke, D. Blaschke, Eur. Phys. J. A **50**, 17 (2014). <https://doi.org/10.1140/epja/i2014-14017-x> [arXiv:1309.6934](https://arxiv.org/abs/1309.6934) [nucl-th]
82. J.P. Blaizot, Phys. Rep. **64**, 171 (1980). [https://doi.org/10.1016/0370-1573\(80\)90001-0](https://doi.org/10.1016/0370-1573(80)90001-0)
83. D.H. Youngblood, H.L. Clark, Y.W. Lui, Phys. Rev. Lett. **82**, 691 (1999). <https://doi.org/10.1103/PhysRevLett.82.691>
84. S. Shlomo, V. Kolomietz, G. Colò, Eur. Phys. J. A **30**, 23 (2006). <https://doi.org/10.1140/epja/i2006-10100-3>
85. J.R. Stone, N.J. Stone, S.A. Moszkowski, Phys. Rev. C **89**, 044316 (2014). <https://doi.org/10.1103/PhysRevC.89.044316> [arXiv:1404.0744](https://arxiv.org/abs/1404.0744) [nucl-th]
86. S. Burrello, M. Colonna, F. Matera, Phys. Rev. C **89**, 057604 (2014). <https://doi.org/10.1103/PhysRevC.89.057604>
87. S. Burrello, M. Colonna, F. Matera, Phys. Rev. C **94**, 012801 (2016). <https://doi.org/10.1103/PhysRevC.94.012801>
88. B.-A. Li, B.-J. Cai, W.-J. Xie, N.-B. Zhang, Universe **7**, 182 (2021). <https://doi.org/10.3390/universe7060182> [arXiv:2105.04629](https://arxiv.org/abs/2105.04629) [nucl-th]